Quasi-One-Dimensional Flow Method for Nuclear Thermal Propulsion Simulator Design

A Thesis Presented for the

Master of Science

Degree

The University of Tennessee, Knoxville

Ethan Michael Long

May 2022

This thesis is dedicated to my late grandfather, Gale Lancaster. He encouraged my curiosity in engineering at a young age and was a strong supporter throughout my educational career. I will forever appreciate his kindness and guidance. He is missed.

Acknowledgments

I would like to thank my parents, siblings, coworkers, fellow students, and professors who have all been an important part of my academic career and life. I would like to especially thank Dr. Trevor Moeller for his guidance and instruction throughout my time as a graduate student. I would also like to thank Dr. Milt Davis and Dr. Phil Kreth for their assistance and willingness to serve on my committee. I would not have accomplished this work without the support of many people along the way, and I am grateful for all of them.

Abstract

Quasi-One-Dimensional flow methods are commonly used to solve flow situations that have multiple driving influences, i.e. heat transfer, area change, and friction. They hold advantages over other computational fluid dynamics methods due to their much lower computational costs and overall simplicity. Typically, these methods are limited in their ability to solve flows due to the simplifying assumptions used. In this model, a simple heat transfer calculation is combined with NASA's Chemical Equilibrium with Applications to constantly update chemical properties within the simulation. In this thesis, a quasi-one-dimensional model including these additions is developed and applied to a NTP simulator design problem. Together, these modifications allow for more complex flows to be analyzed, including those with multiple gas species. The results of the study compare favorably with analytical flow solutions of verification cases. The combined system analysis shows realistic results and expected flow rates compare well with hand calculations. The level of accuracy is acceptable for initial design studies and trade-off comparisons. The methods utilized here apply to more widespread flow cases as well, with some slight adjustment of the model and assumptions used. This study demonstrates the continued usefulness of generalized flow methods despite the continuously declining cost of processing power. The code and method presented can easily be adapted for use in other design efforts and further research.

Table of Contents

List of Figures

Nomenclature

α_i	injection angle
ΔX	spatial step in X dimension
$\dot{m}$	mass flow rate
$\frac{d}{dx}$	spatial derivative in x
γ	ratio of specific heats
μ	viscosity
ρ	density
$_0$	stagnation condition
$_t$	total condition
A	cross sectional area
A_w	wall surface area
C_p	constant pressure specific heat
D	diameter
D_h	hydraulic diameter
f	friction factor
F_D	drag force

G	generic function
g_0	standard acceleration of gravity
h	convection coefficient
I	impulse
I_{sp}	specific impulse
k	thermal conductivity
M	Mach number
mw	molecular weight
P	pressure
Pr	Prandtl number
q	mass specific heat transfer
R	universal gas constant
r_i	injection angle coefficient
Re	Reynolds number
s	entropy
T	temperature
T_c	core temperature
V	velocity
V_i	injection velocity
x	axial coordinate

Chapter 1

Introduction

On July 24th, 1969, the first human set foot on the moon. It was the culmination of years of work and scientific advancement. The event marked both NASA's greatest triumph and the beginning of the end for their golden age. While much progress has been made in the decades since, all manned spaceflight has been limited to low earth orbit since Apollo 17 in December of 1972. Despite what would come of things, plans were made during the Apollo program for an even more ambitious mission out to Mars [1]. NASA knew even its mighty Saturn V would not be able to support such a long-distance mission, so research was being completed to develop a new type of rocket, one that could send a useful load all the way past the moon and into Martian orbit. The primary difference was in the third stage propulsion system, which was planned to be a type known as a nuclear thermal rocket, or NTR. Unfortunately, this project was shelved along with the Mars mission during the post-Apollo budget cuts.

Only recently has the political will and technology changed such that a Mars mission is a possibility once more. With this new push from NASA, nuclear thermal propulsion (NTP) technology is once again being looked at as a possible solution to the difficulty of transporting man and material over interplanetary distances. However, the testing and design work done with operational reactors before the early 1970's in open-air environments cannot be replicated in the current regulatory and political environment. Therefore, a ground simulator will be necessary to complete risk-reduction experiments without radioactive material present. In order to aid in the design of this novel facility, a design tool has been developed that seeks to represent the flow within the proposed simulator through

generalized compressible flow methods. This thesis focuses on that tool, its development, and the proposed facility design.

1.1 Motivation for NTP Systems

Since the 1970's, huge strides have been made in conventional liquid-fueled rockets. These improvements have been driven by better design tools, more advanced materials, and lessons learned from experience. The improvements came in the form of increased efficiency, higher thrust-to-weight ratios, simplified construction requirements, and reusability. The RS-25 of the 1980's, also known as the space shuttle main engine, represents a well-designed, reusable and efficient hydrolox engine. In a vacuum, it achieved an I_{sp} of 452.3s, and a thrust-to-weight ratio of 65.9:1. [2]. Specific impulse, or I_{sp}, is a performance measurement for a combined rocket propulsion system that is similar to the fuel mileage in a car. It is a measure of the change in momentum provided by a given mass of fuel.

Even newer engines, like Space Exploration, Inc's Raptor engine, utilize additive manufacturing and novel combustion cycles to achieve high chamber pressures and re-usability [3]. Even oxidizer-rich staged combustion is regularly achieved by US companies, something that was thought to be impossible in the US prior to the fall of the Iron Curtain[4]. However, these strides in engineering are still limited in total efficiency. Chemical rocket engines are limited in performance by the total energy released by combustion, with a maximum practical I_{sp} with conventional designs in the high 400's. Some experimental engines have achieved I_{sp} values above 500s, but the required propellants and design features are so far impractical to use for flight hardware [5].

Nuclear thermal rockets can be designed to deliver much higher performance. Several near-flight-ready solid core nuclear thermal engines were shown to deliver in excess of 800s I_{sp} in the 1970's [6]. This performance increase comes from decoupling the heat input to the propellant from the combustion of the propellant. Instead, the heat source is nuclear fuel, so the molecular weight of the propellant can be reduced to a minimum and heat is limited only by material limits. Both of these factors allow for a higher specific impulse. Figure 1.1 contains a plot comparing thrust, I_{sp}, and power requirements of various space propulsion

systems. While some systems can match or exceed the efficiency from NTP systems, it is easy to see that NTP systems occupy a unique combination of high thrust with high efficiency. This is the reason it is being investigated for future space missions.

Since the first generation of ground-tested NTP systems, advances in materials and nuclear technology have made it possible to push performance even higher. The performance gains from the development of NTR's would not be limited to the 900s range. Knowledge gained from designing and operating first generation solid core engines would enable a new generation of engines to achieve I_{sp} values that seem impossible today, using even more advanced nuclear engine designs [7]. Additionally, the NTP system provides secondary benefits on long missions, specifically as a source of electricity for life support and electric propulsion systems. To put the performance increase in perspective, the minimum one-way transit to time for a 450s engine to Mars, assuming a round trip mission, is approximately 227 days. For an 900s engine, however, the travel time is reduced to 122 days [8]. These calculations assume a mass fraction of 0.07, parking orbit heights of 400km at both planets, and circular orbits for both Earth and Mars. The mass fraction is a ratio between the initial mass of a vehicle before engine start, including all the propellant, and the final "dry" mass of the vehicle after the propellant has been exhausted. The low thrust-to-weight ratios of NTR systems is due to the additional mass of the reactor and shielding when compared to a typical chemical engine, and results in a higher overall dry mass for a given system. However, it has been found that for the thrust-to-weight ratios above 5, little performance is gained in the transfer orbit missions that NTRs are most suitable for [9]. These assumptions are important to reconsider for specific mission planning, but are appropriate for a general comparison of the transfer time. A plot of transit time vs. specific impulse is included below in figure 1.2, from William Emrich, Jr.'s influential textbook on nuclear propulsion [8].

The plot in figure 1.2 demonstrates the trip length advantage that higher values of I_{sp} provide. There are diminishing returns on performance at higher I_{sp} values, but the initial step from chemical to nuclear propulsion changes the mission duration significantly. This reduction in transit time is important for several reasons. First, the reduced travel time means that the vehicle would not need to carry as much heavy food or supplies. Thus, either an overall smaller vehicle could be used, or more mass could be dedicated

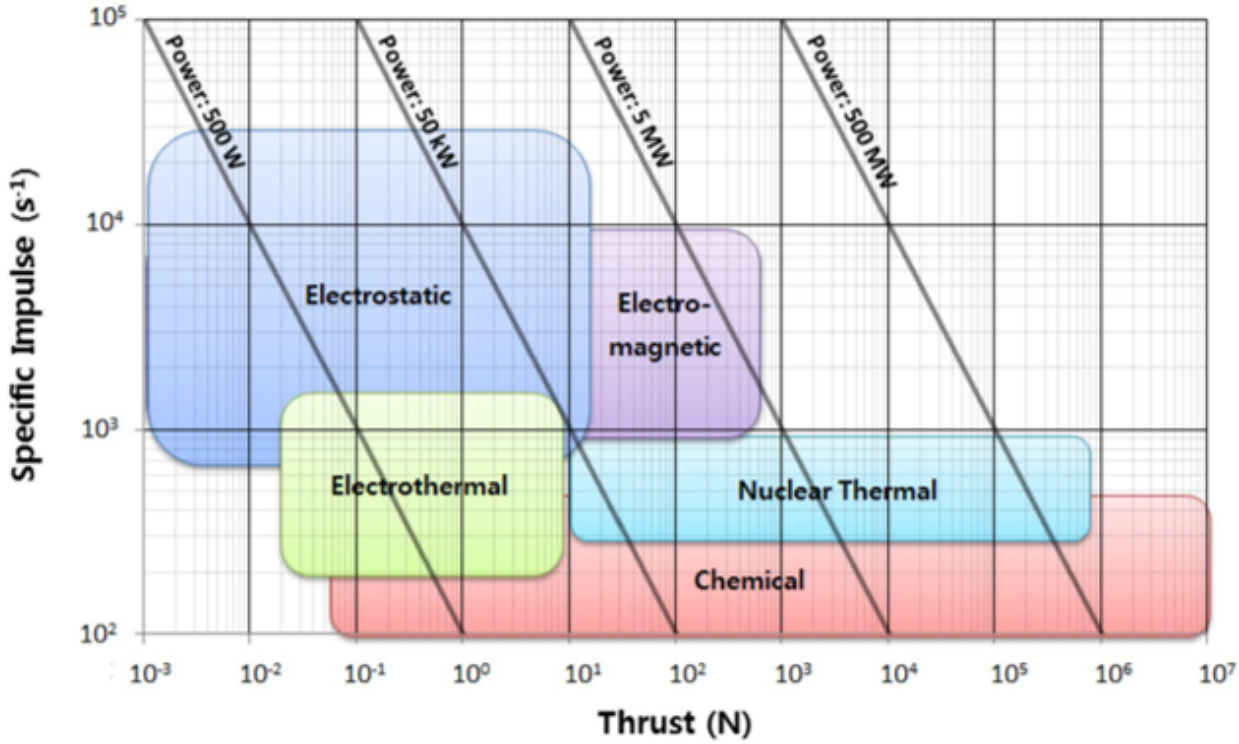

Figure 1.1: Thrust vs. Specific Impulse vs. Power Requirements [10]

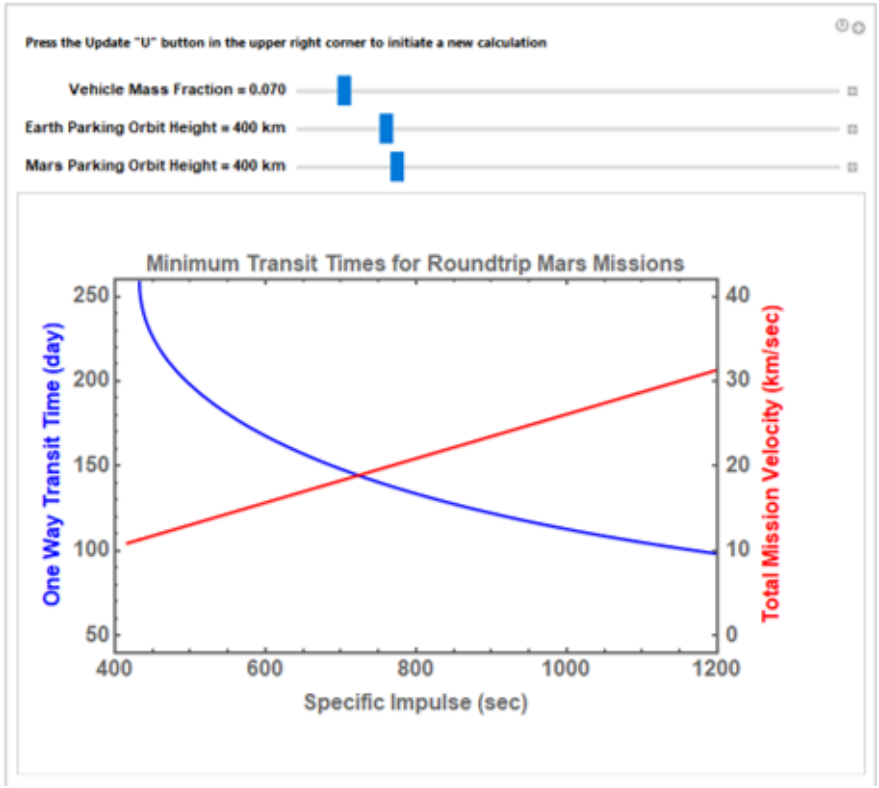

Figure 1.2: One-Way Travel Time vs. Specific Impulse [11]

to scientific payloads. Also, less time outside the protection of an atmosphere means less overall radiation dose, an important consideration for long-duration space missions. These and other advantages can only be properly realized through design and testing of NTR's.

Further efforts to develop the NTP concept after the NERVA program were primarily restricted to design and component-level testing. The largest effort was Project Timberwind, in the 1990's [12]. It was an effort born out of the Strategic Defense Initiative (SDI) program, colloquially called "Star Wars". There was a concern that the Soviet Union may attempt a decapitating nuclear first strike on the United States, so an effort was made to increase ballistic missile defenses. NTR's were looked at as a way to provide the performance necessary to intercept incoming reentry vehicles (RV) during the terminal phase of flight. Incredible performance is required in this stage due to the velocity that the RV's are moving as they reenter the atmosphere. For this program, the turbopumps and fuel elements were the main areas of improvement, both primarily enabled by improved materials [12]. While shifting goals and budget sources hindered the program, it did advance the overall knowledge of NTP rocket design. Since then, most studies completed have been "paper studies", although at least once facility has been created by NASA to study the material properties of potential core components in the high temperature hydrogen environment of the core [13].

There are several challenges associated with this level of performance, however [14]. First, the high temperatures and radioactivity experienced in the core require unique and exotic materials to survive. The heat transfer rates and thermal stresses experienced by both the fuel elements and larger core structure are uniquely high, and expense increases quickly with increased performance. Additionally, nuclear rocket engines have long start-up and shut-down times. Chemical rockets typically start and stop in seconds as propellant is permitted to enter the preburners and the turbopumps spin up, and spin down just as quickly as propellant valves are closed. This simplifies mission planning as the engine burns can be well controlled and time.

Solid core nuclear engines require carefully controlled startups of the reactor core to ensure criticality is reached in an orderly manner [6]. Likewise, shutdown is a slow process and the presence of decay products means that heat must continuously be removed from the system until those products have decayed to stable isotopes [14]. This can be accomplished by

continually pumping propellant through the core and out the nozzle, but this leads to a large loss in efficiency as no appreciable thrust is produced in this mode of operation. Another option is to pass coolant through the core and recapture it to use the waste heat for electricity generation. This process adds complexity and weight to the overall system. Mission planning will also need to account for minimum engine runtimes and the required start-up period. Additionally, the concern of possible radiation leaks would mean that nuclear engines would likely be suitable only for exo-atmospheric operation, with conventional chemical rockets lifting the vehicle through the atmosphere to space. While all of these problems could be addressed with proper engineering, it is still important to consider them when comparing propulsion systems.

1.2 Ground Testing

In the past, testing was completed using operational reactors that mirrored flight systems, with some concessions made for ground support and testing. The exhaust of these test reactors was pure hydrogen, but there was always the possibility of a radioactivity release due to leaking fuel elements. The fuel was highly-enriched uranium (HEU), which was manufactured as particles then cast into fuel rods. To help the fuel survive the harsh operating environment and the effects of hydrogen flows at elevated temperatures, they were coated in a protective ceramic cladding. In normal operation, this cladding would allow heat transfer and heat the flowing hydrogen, while keeping the radioactive elements isolated. However, the large thermal gradient and the uneven expansion between layers of the fuel grains led to cracking and decay products being introduced to the propellant flow. This problem could be solved with more advanced material science, and many companies are looking specifically at the triisotropic (TRISO) fuel developed during project the Space Nuclear Thermal Propulsion (SNTP) project in the 1990's for use in modern reactors. This fuel incorporates several layers of material around a central kernel of uranium for increased strength and temperature resistance. Despite these improvement, the risk of a radiation release remains [8].

Therefore, a non-nuclear analogue would be required for current day testing. The specific solution analyzed in the coming chapters is one in which the fuel rods themselves are replaced with electric resistive heating elements. The specifics of core design and heating element matrix shape would be questions to be investigated by the facility itself, and will be left to later work. For now, the focus is on treating the hot hydrogen effluent that exits the core before it is exhausted to the surrounding environment. There will be no radioactive material in the proposed ground facility, so the treatment will mostly consist of cooling the flow below its autoignition temperature prior to discharge. Limited constraints exist on the design of the downstream cooling systems, so it was decided that a design study of multiple configurations was the best course forward.

Considering this, a design tool was needed for several reasons. First, the rapidly changing nature of the simulator facility design and its requirements meant that the lead time for results needed to be relatively short. Additionally, a lower fidelity design tool can be more appropriate for initial calculations when compared to a more involved computational fluid dynamics (CFD) simulation. Finally, the tool as envisioned offered a "reality check" for the results of higher fidelity methods. The entire system can be modeled relatively easily within the design tool, something that may be prohibitively expensive in computing power or lead time required for a higher-fidelity method. Rapid calculations would allow for rapid results and a more adaptable design. This tool would serve to help remove uncertainty from the design process and to help narrow down the final design targets.

The temperatures and environment that an operational NTP system will operate in require design and verification to ensure it is capable of properly simulating the flight system. The initial conceptual design will be completed using a code based on generalized compressible flow methods. Computational fluid dynamics (CFD) is the typical design tool used for facilities. However, CFD is not without its own limitations. Namely, it remains computationally expensive and time consuming to simulate complex geometries. This is especially true early in the design process when requirements and constraints can rapidly change. In order to aid in the conceptual design process, a faster way to find results in needed. For this reason, generalized flow techniques were investigated.

This thesis follows the following organization. Chapter 2 provides an overview of previous NTP design efforts and applications of quasi-one-dimensional analysis techniques. It serves to frame this thesis within the larger family of work in nuclear thermal propulsion. Chapter 3 contains an explanation of the equations and methodology employed within the design tool. Chapter 4 contains a comparison to analytical solutions of simple flow cases and a study on the effects of a changing step size on the results. Chapter 5 presents the baseline design created for the NTP simulator and offers explanations and analysis of the results found. Finally, Chapter 6 is the conclusion of this thesis and contains suggestions for future work in both the design of the simulator and further refinement of the design tool.

Chapter 2

Background

In the days of the Apollo program, space exploration seemed limitless. NASA had achieved something that seemed impossible just a few years before and had momentum to continue to advance rocketry. The plans laid out for future effort assumed continuing support from the US government, and Von Braun himself planned for a near-future trip to Mars. However, even then there were realistic concerns over budgets and what was achievable. In many minds the Space Race was over when Neil Armstrong set foot on the moon, and the United States had won. The drastic cuts to NASA's budget following this era and the limitations imposed on follow-on projects had a profound effect on the pace of space exploration. Because of these and other factors, humankind has not returned to the Moon for nearly 50 years. But while the Apollo program was still active, work was being done to push past the Earth's sphere of influence. The tool selected for the job was the nuclear thermal rocket.

In liquid rockets, propellants are pumped from tanks, mixed, and burned, producing hot gas that is expanded out a nozzle to produce useful thrust. Two propellant types are required, both an oxidizer and a fuel. The specific compounds selected vary widely, and the mechanism by which they mix and burn also varies, but all bipropellant chemical rockets use combustion to produce thrust. In a nuclear thermal rocket there is only one propellant, typically hydrogen. This hydrogen can be stored as a cryogenic liquid in large tanks before being pumped into the core. A potential operating mode would be the expander cycle, where the cryogenic hydrogen is first pumped around the engine components and nozzle, absorbing heat and boiling. This flow of hot gas is then used to turn a turbine before passing on into

the core. The core of an NTR contains radioactive fuel that is brought to a critical state and decays. The main product of this decay is heat which is released into the fuel elements and the surrounding structure. As the gaseous hydrogen flows through the reactor fuel matrix, it absorbs the heat from the fuel matrix. This brings the gas up to a higher temperature while still at relatively high pressure and low velocity. As the hydrogen exits the core, it is at a state similar to the exhaust gas exiting a chemical rocket combustion chamber. It goes through a similar process after this point, passing through a converging-diverging nozzle to expand the gas and accelerate the flow. It then exits the engine producing thrust. A true flight system would have a much more complicated flow path, but this simplified example gives a good operating overview of the system. An image of a representative system is included in Figure 2.1, below.

2.1 Prior NTP Efforts

Nuclear thermal rockets have seen several periods of interest throughout the last 70 years. Originally seen as an enabling technology for Mars travel, new missions have been considered including the use of nuclear "space tugs" for moving and serving satellites in Earth orbit, or as a potential propulsion system for deep-space probes [15] [1]. Defense related applications have also been investigated and continue to be a possible use case [12]. Regardless of the specific mission, nuclear thermal propulsion would represent a leap in capability and open up new possibilities in space.

2.1.1 NERVA/Rover

Interest in the concept of a nuclear thermal rocket was high in the early atomic age, and two programs were started to support research into the subject. The NERVA program was organized under the Space Nuclear Propulsion Office, a joint effort of the Atomic Energy Commission (AEC) and the nascent National Aerospace and Space Administration, or NASA. NERVA was focused primarily on component-level design and creation of a flight-ready engine. AEC primarily focused on the reactor design and testing under their Rover program, started in 1955. The Los Alamos National Lab handled the AEC effort and led

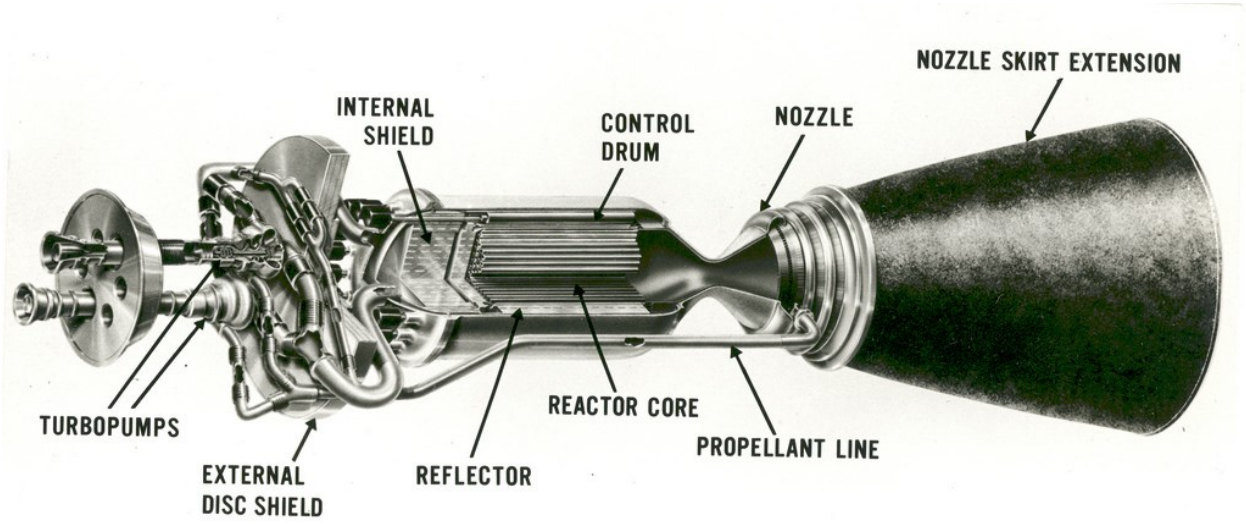

Figure 2.1: Cutaway of a NERVA-type Rocket [1]

construction of a test facility at the Nevada Test Site in 1957, named the Nuclear Rocket Development Station [16]. This site would host all reactor testing done under Rover and NERVA for the next 16 years.

The first test reactor, KIWI-A, was brought online on July 1st, 1959. Following the formation of the Space Nuclear Propulsion office in 1960, the first NERVA engine was tested in 1964. Throughout the program, lessons were learned about fuel grain design and reactor control, among other things. The Phoebus 2-A reactor was the most powerful tested, with a sustained output of 1400MW. The NERVA engines showed incremental improvements, and the XE' engine first tested in 1969 was near-flight ready. This engine was capable of continuous operation at 1100MW of thermal power with "a specific impulse twice that of (a) chemical rocket system [6]." The Rover program also looked at improving ground testing procedures, including a demonstration of a scrubber system to reduce the amount of radiation that was exhausted to the atmosphere.

Challenges came along with success. The main issues encountered in both programs were primarily related to the fuel elements. In a typical water-cooled power reactor, operating temperatures are maintained at a relativity low point, with the sheer mass of water heated providing the high energy transfer required to generate large amounts of electricity. For a space-based system, however, the operating temperature must be much higher [1]. This is primarily a function of the Isp equation, that is, the fuel efficiency of the rocket. In a simplified form, this equation is:

$$I_{sp} = \sqrt{g_0 \frac{R}{mw} T_c} \tag{2.1}$$

The two terms most easily controlled are mw and T_c. The molecular weight, mw, varies based on propellant choice, and is what motivated the selection of hydrogen as the propellant. The other term, T_c, is the operating temperature of the core and must be as high as possible to achieve maximum efficiency. Unfortunately, the high temperatures lead to structural failure of the fuel grains as well. The fuel grains used throughout most of the NERVA/Rover program consisted of uranium oxide particles that were converted to uranium carbide particles and coated in pyrolytic graphite to help contain the fission products within

each fuel particle [8]. These particles were cast into graphite fuel rods, machined to the required tolerances, and loaded into the core. These individual fuel elements were encased in an additional layer of zirconium carbide as well to protect against the corrosive hydrogen atmosphere [1]. Ideally, the graphite inner coating and the zirconium outer layer should have contained decay elements as they were generated throughout reactor operation. However this did not always happen. Instead, the high temperatures and temperature gradients experienced in the core led to cracking in both the graphite fuel element coatings and the zirconium carbide element cladding [17]. Due to this, radioactive material was allowed directly into the propellant flow. As this flow was unfiltered and exhausted directly to the ambient environment, the area around the test cells was irradiated. This was a manageable problem at the Nevada Test Site, where open air testing of nuclear weapons was a common occurrence, but precluded the use of these engines in the first stages of an orbital rocket. This potential radiation problem is part of the reason that full-engine testing has not been completed in the United States since the cancellation of the NERVA/Rover program in 1973 [1].

2.1.2 Project Timberwind and Space Nuclear Thermal Propulsion

The interest in nuclear thermal propulsion was once again reignited during the 1980's, when political motivation returned with the advent of the Star Wars program. The United States was deep in the Cold War and anxiety was high over the possibility of a Soviet nuclear first strike. In order to counter such a threat, the USA began investigating counter-ICBM technology through the Strategic Defense Initiative (SDI) program, colloquially called Star Wars. Several striking proposals came out of the program, but one of particular interest to the topic of nuclear propulsion was project TIMBERWIND. The project investigated the possibility of building high energy, compact nuclear thermal engines with thrust-to-weight ratios much higher than the previous NERVA designs.

The program went through several phases as DOD objectives changed and the SDI program was wound down. At the end, the NTR effort was named the Space Nuclear Technology Program, and in 1991 the design was refocused on potential reusable Air Force applications as opposed to a one-time interceptor use. While the program never

produced a ground test or flight ready vehicle, several small-scale thermal and criticality experiments were completed. The design process addressed problems with the original NERVA program designs and made large improvements in Isp and thrust-to-weight. The greatest advancements were due to the change of core design. Instead of the long solid hexagonal fuel elements used in NERVA designs, TIMBERWIND engines used a particle bed reactor design [12].

In a particle bed reactor, the fuel kernels were similar to the NERVA design of an individual uranium carbide fuel kernel covered in pyrolytic graphite, with the addition of a zirconium carbide layer directly to the kernels. However, these particles were held in a "frit" structure, which allowed for the propellant to pass between individual particles directly. This design massively increased surface area exposed to the flow and therefore allowed for more compact and higher energy density reactors. Efforts were made throughout the program to increase the operating temperature of these particles, and a contract was in place to transfer Russian technology that would have enabled operating temperatures near 3500K. [12] This is not to say that the design was without flaws. For one, the frits that held the particles within the reactors had trouble coping with the thermal gradients and several cracked during testing. Additionally, the thermal gradient issues within the elements themselves were not totally solved, with thermal testing revealing kernel migration within the particles. However, the team was confident that these problems were solvable.

In addition to the improvement of the fuel itself, the material science had come to a level to allow the type of compact, high-performance turbines and turbopumps required for such a system. The strides were primarily made using carbon composites, which were still in their infancy but offered a potential solution once refined. A carbon fiber was developed by the program and used to create both demonstration turbine wheels and an integral pressure vessel and nozzle assembly. Nuclear heating is less of an issue with carbon composites than with typical metals, and this combined with the weight savings made the new fiber an attractive option [12]. Despite the advancements made, the SNTP program suffered from a lack of urgency and political motivation following the collapse of the Soviet Union, and was cancelled in 1992.

Several efforts have explored the possibility of nuclear space propulsion, including both thermal and electric variants, but none have tested hardware to the extent of SNTP since the program's cancellation. A discussion of nuclear thermal propulsion would be incomplete without mentioning work elsewhere. There was research conducted in the Soviet Union to produce a nuclear thermal rocket. While not as well supported as research in the US, efforts there resulted in the creation of the RD-410 engine [18]. This design had several advanced features that allowed it to achieve slightly higher performance than NERVA. Namely, the fuel elements were twisted to increase heat transfer from the fuel to the propellant flow, along with advanced material usage. However, it was never funded to the same extent and was limited in its overall scope. Soviet research in carbides and other material science topics were made available to the international community following the fall of the Iron Curtain, and have been applied to past and current research efforts with good results [8] [12].

2.2 Generalized Compressible Flow as a Design Tool

The advancements above are numerous and significant, but a common challenge is ground testing in a cost-effective manner. Haslett, the head of the SNTP program, cited the ground test facility as a major cost driver of the entire program [12]. These challenges would be especially significant for modern civilian testing, where more public scrutiny increases the risk of backlash and cancellation. These factors pose a large financial and programmatic risk for any potential new reactor design. For these reason, non-nuclear ground testing is proposed as a way to reduce technical risk in the reactor design without running into the difficulties of handling nuclear material. An effort has been made to design a ground-based simulator which would replace the nuclear fuel rods with electrically resistive heating elements. This would allow for reactor core refinement before the introduction of any nuclear material and help reduce the overall risk in the design. Such a facility would be unique, and there are many questions and design values yet to be decided. Because of this, the initial design process needs to be flexible with the ability to rapidly compare multiple design options. This need motivated the creation of a flexible, computationally inexpensive design tool to allow rapid assessment of potential test facility designs.

2.2.1 Development of the Equations

The earliest textbook example of the quasi-one-dimensional flow method was by Shapiro is his 1953 textbook [19]. He proposed the derivation of a set of equations that together could be used to solve the flow state of a gas based on several driving functions, with several constraining assumptions. The specific derivation used in this thesis will be documented in more detail in the following chapter. Several sources address the quasi-one-dimensional methodology. It is the same method used to teach and solve Raleigh flows, isentropic flows, and Fanno Flow, but with the effects analyzed in each combined. That is, friction, change in area, heat addition, and flow injection can all be analyzed at once. The specific derivation and use of these equations will be addressed in further detail in Chapter 3.

2.2.2 Prior Applications

Quasi-One-Dimensional analysis has been used in the past where computing power constraints or calculation speed made it preferable to more complex analysis techniques. These constraints have begun to reduce as more powerful processors have become available, but there continue to be applications of this lower fidelity method. Even with reduced computational costs, computational fluid dynamics still remains a complex field, and accurate mesh generation remains an art, with skilled specialists required to obtain useful results. Conversely, one-dimensional codes can be much simpler to understand and require less set-up effort before obtaining results.

One recent application of a quasi-one-dimensional method was in real-time simulation. In 2011, there was a need for an improved facility model at the Arnold Engineering Development Complex (AEDC) in Tullahoma, TN [20]. The facility hosts many large and unique wind tunnel facilities, and had digital models to help train operators and test out control systems prior to implementation. However, the existing model relied on a lumped parameter method, and didn't account for various real-world factors that affected the flow. These included heat transfer, minor losses to friction, and changes in area. Brett Boylston, an engineer at AEDC, worked to update the model using a quasi-one-dimensional method based on Shapiro's methods [20]. The updates were implemented through a Simulink model, then

transferred to C++. This change from an interpreted to a compiled language led to a calculation speed that enabled real-time simulation of the facilities. Boylston [20] verified by comparing the results with classical solutions for each driving function in isolation, and saw good results when implemented. It was found that the lumped-parameter method had over-predicted mass flow by as much as 35%. The improved model enabled better training and more realistic testing of control systems [20].

One-dimensional models have been used as a design tool for decades. Beans [21] wrote a paper describing a numerical solution to Shapiro's equations in 1970. He includes a suggested method to solve different flow regimes and analyzes some basic flows using his code [21]. Following this, he wrote of a potential application for this method in 1992 [22]. This paper describes the use of one-dimensional methods in nozzle design as an alternative to Rao's Method of Characteristics and more complex, multi-dimensional analysis. Beans highlights the method's usefulness as a design tool, especially in comparison of relative difficulty and computational expense [22].

One potential design application is in supersonic flows. In 2009, Birzer and Doolan investigated the use of one-dimensional methods in the design of a hydrogen-fueled scramjet [23]. They created a quasi-one-dimensional model using the typical method, but modified their resulting model to incorporate a chemical equilibrium and mixing length calculations. This enabled their updated code to calculate the performance of a hydrogen-fueled combustor design. They had three experimental sources of data to compare with, and found good agreement in the results. This supported the continued use of this method for design [23].

Picard et al. applied a one-dimensional method to turbomachinery analysis [24]. By changing the frame-of-reference, the flow between sections within a rotary-ramjet engine can be analyzed as one-dimensional. The specific implementation accounted for shocks, heat transfer to the turbine, heat addition from combustion, area change, and friction. The baseline design made with the help of the design tool was manufactured and tested in a proof-of-concept experiment. The results of this test showed good agreement, with the largest inconsistency caused by a difference in friction between the smooth computational model and actual manufactured device [24].

More examples exist of one-dimensional analysis techniques. The studies listed above are highlighted in particular for their reliance on the very same equations used in this work. Various modifications have been made to handle unique design situations, but the adaptability and applicability of quasi-one-dimensional flow analysis has been shown previously. The work that follows is a continuation of prior efforts and will seek to demonstrate the usefulness of this method for a nuclear thermal propulsion simulator design.

Chapter 3

Methodology

The first mention and work on a generalized compressible flow method was made in 1953 by A. H. Shapiro in his textbook, The Dynamics and Thermodynamics of Compressible Fluid Flow [19]. This book outlined the derivation process of the equations used in this method, but did not provide a numerical solution method. The methods are discussed in further textbooks by Saad [25] in 1985, and Zucrow and Hoffman [26] in 1976. Additionally, Beans described a potential use of such a method in his 1992 paper, "Nozzle Design Using Generalized One-Dimensional Flow [22]." B. K. Hodge was the first to detail a computational solution method and provide an example program in his 1991 paper on the subject entitled, "Generalized One-dimensional Compressible Flow Techniques" [27]. This paper and its supporting references provide the theory that is at the core of the present work. Modifications have been made to operate in a more modern language and to handle more complex problems.

The Quasi-One-Dimensional technique comes from the same equations taught in many compressible flow courses. The main relations used throughout are similar as is the underlying assumption that the flow is dominated by flow in one direction, steady state, and the fluid is a perfect gas. The conservation laws are a common starting point. Anderson's textbook on compressible flow is often used in courses on the subject, and provides derivations of relations for Rayleigh Flow, Fanno Flow, and Isentropic Flow [28]. All have a common starting point, the equations for conservation of mass, conservation of momentum, and conservation of energy [28]. However, each of these unique cases assumes that only one factor is affecting the flow. For Rayleigh this is heat addition, friction for Fanno flows, and

a change in area for Isentropic flows. For many flow cases, one of these factors will dominate and the relevant flow case will be applicable. However, it is possible to analyze the combined influence of all the factors if these assumptions are not made, at the expense of increased computational cost and complexity. This combined analysis is called a quasi-one-dimensional analysis. For the remainder of the discussion, the "quasi-" is implied and will be dropped from the name. The particular equations and methods employed in this type of analysis are discussed below.

3.1 Derivation of Equations

The derivation of the quasi-one-dimensional relations begins with an equation of state. Several textbooks detail the derivation, including those by Saad [25], Zucrow and Hoffman [26], and Hodge and Koenig [29]. A brief review is included here, following the method as described by Saad [25]. A representation of the control volume analyzed is included in figure 3.1, from Zucrow and Hoffman's textbook on gas dynamics [26].

The equation of state used is the perfect gas law, relating pressure, temperature, and density. This equation requires that the heat capacity of the gas is constant, and that the fluid analyzed behaves as an ideal gas. This assumption is accurate as long as the gas is not at especially low temperature or pressure.

$$p = \rho RT \tag{3.1}$$

Throughout the derivation, a technique is used to non-dimensionalize and simply the calculations. This is explained by Hodge and Koenig [29], and consists of taking the natural log of each relation and then differentiating it in terms of x. Using the equation of state as an example, taking natural log results in the form of

$$\ln p = \ln \rho + \ln R + \ln T \tag{3.2}$$

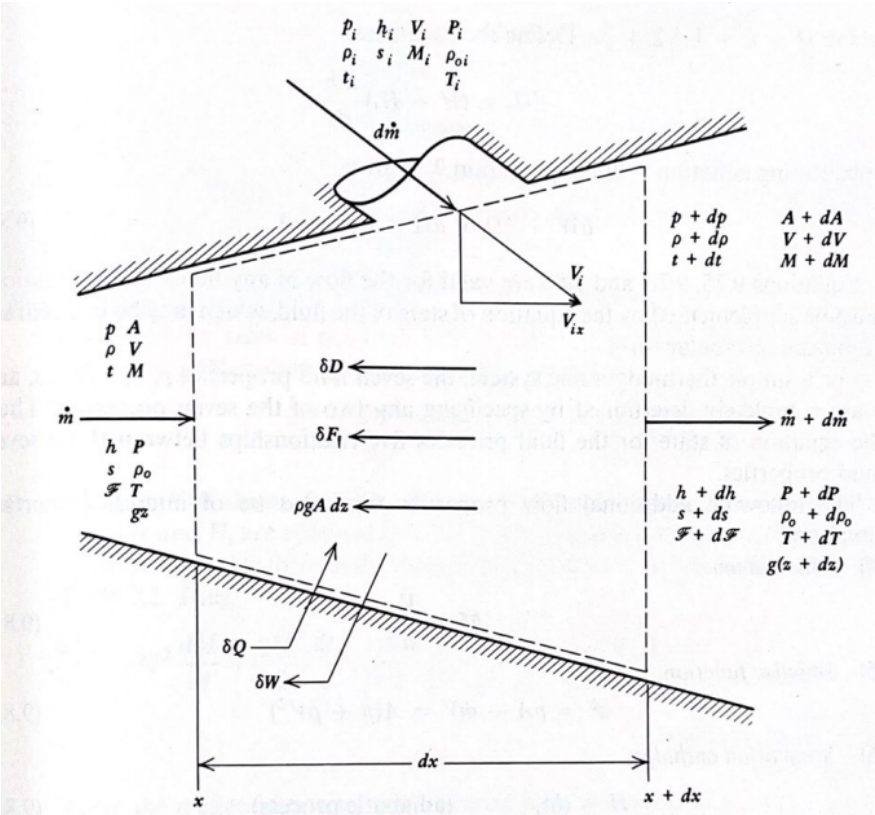

Figure 3.1: Representative Control Volume [26]

Then differentiating in terms of x,

$$\frac{dp}{p} = \frac{d\rho}{\rho} + \frac{dT}{T} \tag{3.3}$$

All the equations presented below will be in this form.

Applying a similar technique to the definition of Mach number and squaring yields

$$\frac{dM^2}{M^2} = 2\frac{dV}{V} - \frac{dT}{T} \tag{3.4}$$

The purpose of the use of M^2 as opposed to M term is to simplify the later analysis.

From the continuity equation,

$$\frac{d\dot{m}}{\dot{m}} = \frac{d\rho}{\rho} + \frac{dA}{A} + \frac{dV}{V} \tag{3.5}$$

The conservation of energy is a bit more complex. The derivation requires neglecting higher-order terms but a relationship can be found that relates the change in stagnation temperature to heat, work, and stagnation-enthalpy terms. Again, this relation assumes that the heat capacity is constant. Using the definition of Mach number again, it can be shown that

$$\frac{dT_0}{T_0} = \frac{dT}{T} + \frac{\frac{\gamma-1}{2}M^2}{1+\frac{\gamma-1}{2}M^2}\frac{dM^2}{M^2} \tag{3.6}$$

The conservation of momentum equation requires the introduction of relations for shear stress:

$$\tau_w = f\frac{\rho V^2}{2} \tag{3.7}$$

wall area:

$$dA_w = \pi D dx \tag{3.8}$$

injection angle:

$$\frac{V_i \cos\alpha_i}{V} = r_i \tag{3.9}$$

and the following relation between velocity and Mach number:

$$\rho V^2 = \gamma p M^2 \tag{3.10}$$

This reduces the original momentum equation to the following form:

$$\frac{dp}{p} + \frac{\gamma M^2}{2}\left(\frac{4f\,dx}{D} + 2\frac{dX}{\gamma p A M^2} - \frac{2\,\Sigma\, r_i\, d\dot{m}_i}{\dot{m}}\right) + \gamma M^2 \frac{dV}{V} + \gamma M^2 \frac{d\dot{m}}{\dot{m}} = 0 \tag{3.11}$$

The one-dimensional analysis also includes an impulse function,

$$\frac{dI}{I} = \frac{dp}{p} - \frac{dT}{T} \tag{3.12}$$

the second law of thermodynamics,

$$\frac{ds}{c_p} = \frac{dT}{T} - \frac{\gamma - 1}{\gamma}\frac{dp}{p} \tag{3.13}$$

and the definition of stagnation pressure.

$$\frac{dp_0}{p_0} = \frac{dp}{p} + \frac{\frac{\gamma M^2}{2}}{1 + \frac{\gamma - 1}{2} M^2}\frac{dM^2}{M^2} \tag{3.14}$$

Together, these eight equations contain the following twelve variables:

$$\frac{dp}{p}, \frac{d\rho}{\rho}, \frac{dT}{T}, \frac{dM^2}{M^2}, \frac{dV}{V}, \frac{d\dot{m}}{\dot{m}},$$

$$\frac{dA}{A}, \frac{dT_0}{T_0}, \frac{dI}{I}, \frac{ds}{c_p}, \frac{dp_0}{p_0},$$

and

$$\left(\frac{4f\,dx}{D} + 2\frac{dX}{\gamma p A M^2} - \frac{2\,\Sigma\, r_i\, d\dot{m}_i}{\dot{m}}\right)$$

If the following four independent variables are either known or defined,

$$\frac{dA}{A}, \frac{dT_0}{T_0}, \left(\frac{4f\,dx}{D} + 2\frac{dX}{\gamma p A M^2} - \frac{2\,\Sigma\, r_i\, d\dot{m}_i}{\dot{m}}\right), \frac{d\dot{m}_i}{\dot{m}}$$

then the system can be solved.

It should be noted that these equations and assumptions must only be valid within each individual control volume in the flow. That is, they hold across each dx increment of the flow. An assumption of constant properties across each increment must be made, but will be valid across sufficiently small values for dx. A sensitivity study was completed to demonstrate and validate this concept, the results of which are included in Chapter 4. Equations 3.1 - 3.14 are useful, but a solution method must be used in order to arrive at a result.

3.2 Numerical Integration

The general solution technique for the above system of equations is through a numerical integration. The domain is discretized into individual control volumes of length, dx, and height defined by the geometry. For the purposes of this method, the geometry is assumed to be axisymmetric. Hodge provides an example of a computer program used to solve the system of equations numerically in his 1991 paper on the subject [27]. He first defines the differential equation to be solved in terms of Mach number as,

$$\frac{1}{M^2}\frac{dM^2}{dx} = \frac{\psi G(x,\gamma,M)}{1-M^2} \tag{3.15}$$

With ψ defined as

$$\psi = 1 + \frac{\gamma - 1}{2} \tag{3.16}$$

and

$$G(x,\gamma,M) = -2\frac{1}{A}\frac{dA}{dx} + \gamma M^2\frac{4f}{D} + (1+\gamma M^2)\frac{1}{T_0}\frac{dT_0}{dx} + 2(1+\gamma M^2)\frac{1}{\dot{m}}\frac{d\dot{m}}{dx} \tag{3.17}$$

An assumption has been made concerning the injection angle of the mass flow, setting it perpendicular to the flow. Additionally, induced drag is neglected, leaving wall friction as the only drag force. With these assumptions the equation above relates the four driving

functions accounting for the effects of area change, friction, mass injection, and heat addition to the change in the local Mach number of the flow.

The 4^{th} order Runge-Kutta method is implemented in the solution process. For this work, the equation to be integrated, from Hodge[27], is

$$\frac{1}{M^2}\frac{dM^2}{dx} = \frac{\psi G(x,\gamma,M)}{1-M^2} \tag{3.18}$$

Here, ψ, defined in equation 3.19 is a term used to make the equation more compact, and is defined as

$$\psi = 1 + \frac{\gamma - 1}{2} \tag{3.19}$$

The function $G(x,\gamma,M)$ is a function of the position in the x, or streamwise direction, the ratio of specific heats γ, and Mach number. The four driving functions included in the equation are as follows:

$$G(x,\gamma,M) = -2\frac{1}{A}\frac{dA}{dx} + \gamma M^2\frac{4f}{D} + (1+\gamma M^2)\frac{1}{T_0}\frac{dT_0}{dx} + 2(1+\gamma M^2)\frac{1}{\dot{m}}\frac{d\dot{m}}{dx} \tag{3.20}$$

The terms of the above equation account for the change in area $\frac{dA}{dx}$, the effect of friction $\frac{4f}{D}$, the change in total temperature $\frac{dT_0}{dx}$, and the injection of mass $\frac{d\dot{m}}{dx}$, respectively. By defining these four driving functions, the equation 3.20 can be solved for Mach as a function of axial position throughout the problem geometry. Changes in other flow properties are found using integral relations. These are as follows, also by Hodge [27]:

$$\frac{T_2}{T_1} = \frac{T_{0_2}}{T_{0_1}}\frac{1+\frac{\gamma-1}{2}{M_1}^2}{1+\frac{\gamma-1}{2}{M_2}^2} \tag{3.21}$$

$$\frac{P_2}{P_1} = \frac{\dot{m}_2 A_1 M_1}{\dot{m}_1 A_2 M_2}\sqrt{\frac{T_2}{T_1}} \tag{3.22}$$

$$\frac{V_2}{V_1} = \frac{M_2}{M_1}\sqrt{\frac{T_2}{T_1}} \tag{3.23}$$

$$\frac{\rho_2}{\rho_1} = \frac{P_2}{P_1}\frac{T_1}{T_2} \tag{3.24}$$

$$\frac{P_{0_2}}{P_{0_1}} = \frac{P_2}{P_1}\left[\frac{T_{0_2}}{T_{0_1}}\frac{T_1}{T_2}\right]^{\frac{\gamma}{\gamma-1}} \tag{3.25}$$

$$\frac{\Delta s}{c_p} = \ln\frac{T_2}{T_1} - \frac{\gamma-1}{\gamma}\ln\frac{P_2}{P_1} \tag{3.26}$$

In this manner, the combined effects of the driving functions on the flow state are calculated and the flow state can be found throughout a given problem. The above explanation follows closely with Hodges work, who originally proposed the method for use in educational settings and provided an example code. His solution procedure is based on the work of Zucrow and Hoffman for shockless flows [26]:

1. Define the initial conditions and the driving functions
2. Integrate from x to $x + \Delta x$ using Runge-Kutta
3. Calculate physical properties at $x + \Delta x$
4. Repeat iteration throughout the problem geometry until $x = x_{max}$

Hodge also provides example problems and results to help readers understand the implementation of such a code. There are ways provided to use this method in flows that contain shock waves. However, for the design problem analyzed here, no shocks are expected and the shock handling is neglected for simplicity. The motivation of Hodge's work was to provide a method for students to analyze more complex flows and to better understand the effects each driving function has on the overall flow state. Accordingly, the specific implementation of Hodge assumes a constant friction factor, detailed knowledge of the change in total temperature, and equation-defined geometry and mass inflows. Additionally, the example code provided was written in MS-DOS, which is not widely used today. The work that follows details the modifications and improvements made in the present work to make a more applicable design tool for the nuclear thermal simulator design problem.

3.3 Driving Functions

The prior work assumes that each driving function is defined by an equation as a function of x, and that the differential is easily found by taking the first derivative of the equation. However, this may not always be the case. For design problems specifically, the driving functions may only be defined at discrete points, and the change in properties between each point must be determined another way. This is typically done through interpolation. For properties that are not necessarily known ahead of time, such as heat transfer, the driving function must be defined differently. These relations will accurately model the effects of each driving function on the flow within either a fully supersonic or subsonic case. Near the sonic point, where the Mach number is equal to one, the solution process diverges. This behavior can be corrected with the addition of a relation that "smooths out" the iteration process through the sonic point by progressing at a constant Mach number increment. However, this method has not been implemented for this specific tool for simplicity.

3.3.1 Area Change

The first driving function addressed is the effect of a changing flow area. This is dictated by the geometry, which must be known or at least assumed within the problem statement. Assuming that the geometry is available as a list of x and y coordinates, the area at each position can be calculated. The geometry is assumed to be axisymetric, so the y coordinate is taken as a radius and the cross-sectional area is calculated accordingly. To arrive at a derivative, the central difference method is employed, the formula representation of which is

$$\frac{dA}{dx} = \frac{A_{x+\Delta x} - A_{x-\Delta x}}{2\Delta x} \tag{3.27}$$

The first and last cells use a forward and backward difference method, respectively. The derivatives are then multiplied by the cross sectional area at each value of x. The values of area between defined points are found using MATLAB's built in *interp1* function.

3.3.2 Friction

Friction is the second driving function. Prior to simplifications, the form of the friction driving function is

$$\frac{4f}{D_h} + \frac{1}{\gamma PAM^2}\frac{dF_D}{dx} - 2r_i\frac{1}{\dot{m}}\frac{d\dot{m}}{dx}$$

with the injection angle coefficient,r_i, defined as

$$r_i = \frac{V_i \cos\alpha_i}{V} \tag{3.28}$$

α_i is the angle between the main flow and the injected flow. This equation can be simplified by assuming that the flow injection is perpendicular to the flow, which means that $\alpha_i = 0$ [29]. Additionally, the term F_D is meant to account for the additionally sources of drag generated by objects within the control volume. However, only wall friction is accounted for in this application, so the driving function simplifies to the form

$$\frac{4f}{D_h}$$

While the hydraulic diameter D_h can be found from geometry, the value of the Fanning Friction Factor,f must be determined through the use of correlations. Here, the Petukhov's relation for the Darcy Friction Factor for fully developed, turbulent flow is used. It must be modified to calculate the Fanning Friction factor, which is simply $\frac{1}{4}$ the Darcy Friction Factor. Therefore, it can be found using the following relation [30]:

$$f = \frac{1}{4}(0.790\ln Re_D - 1.64)^{-2} \tag{3.29}$$

Here, Reynolds number is defined as

$$Re = \frac{4\dot{m}}{\pi D\mu} \tag{3.30}$$

The inclusion of Reynolds number in equation 3.30 presented new unknowns. A value for viscosity must be calculated at each iteration as the temperature varied. This problem was

one of the motivations behind the inclusion of a chemical equilibrium solver named Chemical Equilibrium with Applications for Matlab (CEAM) in the tool, which is covered further in section 3.4.1.

3.3.3 Heat Transfer

Heat transfer out of the flow has a large effect on the flow state and is one of the biggest design concerns faced. For the nuclear thermal simulator, large temperature gradients will drive high heat loads that must be effectively transferred to a heat sink. This could possibly take the form of a cooling circuit that dumps into a nearby man-made lake originally created for the purpose of cooling large wind tunnels at AEDC [31]. Alternatively, a large thermal mass of water stored in a tank could be used due to the limited run time of the facility. Regardless, the heat transfer to the wall is what is important for the flow calculation. The heat transfer is reflected in the flow as a change in total temperature, found here as

$$\Delta T = q/c_p \tag{3.31}$$

where

$$q = hA_s(T_{wall} - T_{flow}) \tag{3.32}$$

and

$$Nu_{D_h} = \frac{hD_h}{k} \tag{3.33}$$

The variable of Nu_{D_h} is Nusselt Number, which is a ratio between convection and conduction heat transfer. This value is typically found using relations based on empirical data. Here, the Gnielinksi correlation is used due to its applicability to a wide range of flow conditions, including $0.5 \leq Pr \leq 2000$ and $3000 \leq Re_{D_h} \leq 5e6$ [32].

$$Nu_{D_h} = \frac{(f/8)(Re_{D_h} - 1000)Pr}{1 + 12.7(f/8)^{1/2}(Pr^{2/3} - 1)} \tag{3.34}$$

In equation 3.34, f is the Darcy (or Moody) Friction Factor, not the Fanning Factor defined previously. Therefore, the unmodified form of Petukhov's relation can be used, lacking the $\frac{1}{4}$ factor. An assumed wall temperature is the last value required to calculate the heat transfer and the change in total temperature within each differential volume. In the future, the wall temperature could be tied to an energy balance between the cooling flow for the wall and the heat flux in, but that has not been implemented in the current version.

3.3.4 Mass Injection

Mass injection is the fourth and final driving function considered. Again, the form of the independent variable in this equation is $\frac{1}{\dot{m}}\frac{d\dot{m}}{dx}$, where both the injection mass flow, $\dot{m}$, and the first derivative of that value as a function of x, $\frac{d\dot{m}}{dx}$, must be known at each point. A method similar to that used for area is applied to the mass injection, with a central difference method used to find the derivative. Again, MATLAB's *interp1* is used to interpolate between defined values.

3.4 Modifications

The methodology explained thus far provides a way to solve a variety of flow problems. However, there remains several problems to solve. First, a method for finding chemical properties of the flow gas must be found. Viscosity, heat capacity, and other values change based on the local temperature of the flow. Equations exist to calculate these individually, but it would be a complex process to implement for every cell in every iteration. Additionally, a method must be found to calculate the properties of a gas mixture, specifically in the portions of the flow that include wall injection of a different gas species. As mentioned above, the tool has been modified to accept a series of discretely defined points instead of a continuously-defined equation for area and mass injection. The combined result of these changes broaden the problems and cases to which the design tool is applicable.

3.4.1 Chemical Equilibrium with Applications

In order to calculate the necessary values for viscosity, density, heat capacity, the ratio of specific heats, and molecular weight of the gas, a program called Chemical Equilibrium with Applications (CEA) was integrated with the design tool [33]. CEA provides a chemical equilibrium calculation based on knowledge of the species, temperature, and pressure of the gas mixture. The specific mechanism by which it works is explained in detail in the user manual, written by B. McBride and S. Gordon, who are also the original authors of the code [34]. CEA has been ported to several languages, including MATLAB. The MATLAB port is known as CEAM, and was used in the present tool, due to the ease with which it can be called and the results used for future iterations [35].

3.4.2 Multi-Species Flow

The addition of CEAM enables the analysis of multi-species and high-temperature flows. In the simulator, cooling gas will be injected downstream of the core. The properties of the resulting mixture can be found using CEAM, in a similar manner to that of the single-flow problem. Instead of a combined temperature definition, the input gas temperature and mass flow is individually defined. CEAM then calculates the resulting gas properties at the location $x + \Delta x$ and uses those for the following iteration. For mixing flows, special consideration must be made to accout for the heat transfer into the flow that occurs as the mass is injected. In order to manage both of these factors, the design tool accounts for the area within each volume used for mass injection and the area that will be at the wall temperature. The gas injection is assumed to occur at the same pressure as the primary flow. The heat transfer out of the flow and resulting reduction in total temperature is accounted for using the properties of the main flow initially. The resulting temperature of the primary flow is then used as an input into CEA and combined with the incoming gas to find the final conditions at the exit of each differential cell. This is a conservative calculation for cooling, as the temperature of incoming gas will be lower than that of the cooled walls. Thus, the required cooling flow will be lower than what is found using this method. Therefore, this can be considered an upper-bound estimate for the required cooling.

3.4.3 Other Considerations

The design tool must address several questions unique to the nuclear thermal simulator. One of these is the pressure differential that must exist between the upstream core and downstream exhaust stack, which exits to ambient atmospheric pressure. This differential must match the conditions present in a flight engine, where it is created by the nozzle. However, the ground simulator is not concerned with generating thrust and must create a pressure drop in another way. A potential solution would be a pressure regulator, however the required inlet temperature is well above what is possible with such a valve. Instead, the pressure differential will be created with a series of orifice plates in this system.

Backpressure orifices are typically used to limit the rate of release of hazardous gases if valves or piping fail [36] [37]. The principle of operation is similar to that of an orifice flow meter, where the pressure drop generated by the restriction in diameter is used to determine the mass flow rate through the pipe. Unlike a flow meter, however, the goal of the restriction orifice is to maximize the friction losses in the system. For the purpose of this problem, the orifice is modeled in isolation, with only the upstream flow conditions from the iterative solution used in the calculation.

Chapter 4

Verification and Validation

Validation of results with known solutions is an important step for any new or novel flow analysis technique. While the underlying theory of the design tool has been applied to many techniques and verified in the past, the specific implementation and inclusion of CEAM in this tool required new validation tests. The results of the tool were compared against analytical solutions available to analyze flow with one driving function in isolation. Minor modifications had to be made, such as setting the friction factor or heat transfer constant, in order to conduct the verification tests. However, as long as the method used to find the true friction factor and heat transfer rates is in itself valid, then the overall method should also be valid. By using standard relations to find these individual values, the integrity of the larger solution is ensured.

In addition to the comparison with the known solutions, a mesh dependence study was conducted to determine what values for Δx eliminate grid dependence and are appropriate to arrive at an accurate solution. The number or iterations has the largest effect on the overall code execution time, as CEAM must be called and the flow calculations run for each individual cell. In order to keep the execution time reasonable, the value of Δx must be as large as possible, while still capturing the changes in flow accurately.

4.1 Comparison with Theory

The quasi-one-dimensional analysis method allows for the analysis of the combined effects of multiple driving factors on a flow. These factors can be analyzed and solved for analytically if considered in isolation. Therefore the design tool was compared to the analytical solutions of each individual driving function for a given geometry.

4.1.1 Flow with Area Change

The first case compared against was that of isentropic flow. Here, only a change in flow area should contribute to a change in Mach number, and therefore, a change in flow state. It is assumed that both friction and heat transfer are negligible, and chemical properties of the flow are constant throughout. For this case, a geometry was generated that included a $2m$ long section of $1.0m^2$ cross-sectional area, followed by a $3m$ contraction section, and ends with a $5m$ long constant-diameter section with a cross-sectional area of $0.5m^2$. The geometry is shown below, in figure 4.1. The working fluid was air, with an inlet total temperature of $T_0 = 273K$, a total pressure of $P_0 = 101.3kPa$, and an inlet Mach number of $M = 0.05$. The low Mach number was used to demonstrate the applicability of the method to the low velocity conditions expected in the simulator. A plot of the Mach number predicted by the code compared to the analytical solution is presented in figure 4.2. The number of points plotted from the design tool solution was limited to make the plot easier to read. The error for each point, compared to the "true" value as found analytically, was calculated according to the error formula, equation 4.1.

$$\%error = \frac{|M_{predicted} - M_{true}|}{M_{true}} \times 100\% \tag{4.1}$$

Using this method, the average error for this case between the values predicted by the analytical solution and the design tool was less than 0.01%. The low error supports the conclusion that the individual driving functions are still modeled correctly within the larger design tool. The equation solved simplifies out to be the same as the area change formula in isolation, so this behavior is expected. The addition of CEA was also seen to not have a large affect on this particular test, as no heat transfer is modeled so the property calculation

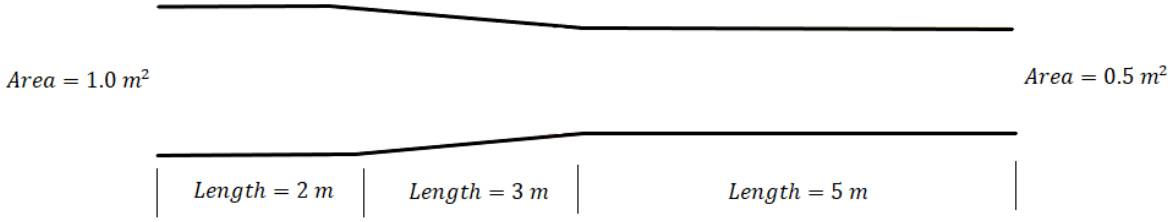

Figure 4.1: Geometry for Isentropic Flow Test Case

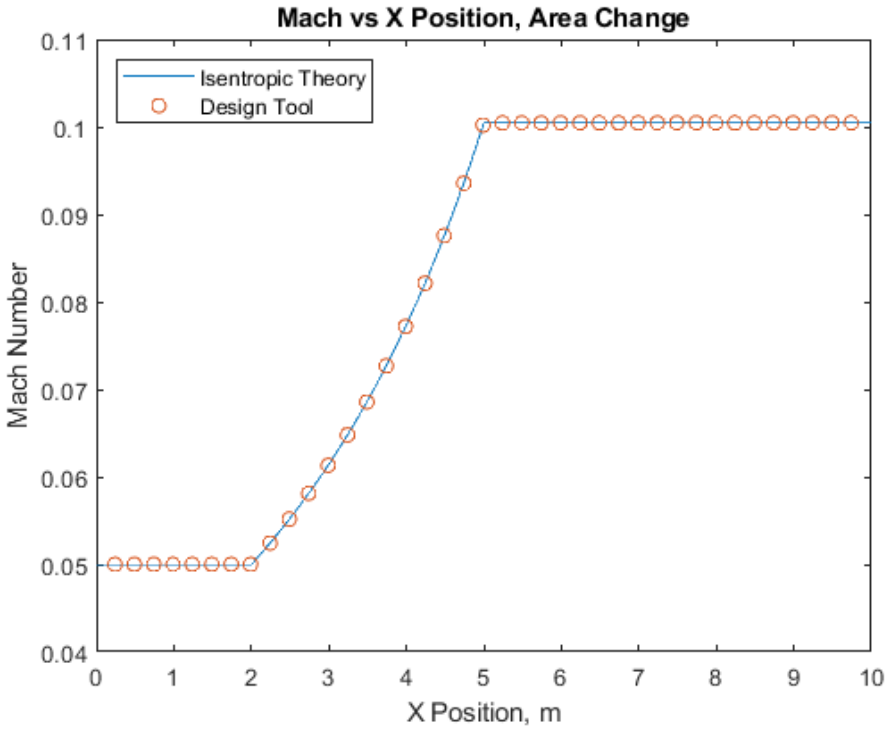

Figure 4.2: Mach vs. X Position, Simple Area Change

do not play a role in the solution. The results help verify the lack of any adverse effects from the changes on the area calculation.

4.1.2 Flow with Heat Addition

The second driving function to be analyzed in isolation was heat addition, known as Rayleigh flow. The geometry for this case is a constant-area pipe, with the flow assumed to be frictionless. The heat transfer to the flow was assumed to occur at a constant rate of $1e5 W/m$ throughout the geometry. The pipe was $10m$ long with a cross-sectional area of $0.5m^2$. An image of the geometry is included in figure 4.3. For this case, a Δx of $0.01m$ was used for both the theory and design tool solutions. The entry conditions were a total temperature of $273K$ and an inlet total pressure of $101.3kPa$, with the entry Mach of $M = 0.05$. The design tool was run for two different cases, the first with an assumed heat capacity of $C_p = 1005 J/kgK$. The second case employed CEAM to calculate the value of C_p as it changed with temperature.

The two solutions are plotted against the values found using the Rayleigh flow equations in figure 4.4. This comparison demonstrates a strength of the design tool, namely the ability to account for changing properties of the flow. The solution with CEAM enabled varies more from theory than the assumed C_p case, as expected. The difference is relatively small for the low temperatures of the test case, but the difference is more pronounced at the high operating temperatures present in the NTP simulator. This is because the change in heat capacity is more pronounced at elevated temperatures, especially once dissociation begins to occur. This process significantly changes the effective heat capacity of the fluid.

The average error was calculated as before for both cases. When the value of C_p was held constant, the error was 0.29%, while the error increased to 0.54% for the case with CEAM enabled. The outlet temperatures also varied by $138K$, with the constant C_p case predicting an outlet temperature of $1268K$, while the CEAM case predicted an outlet temperature of $1130K$. This is a significant difference when considering heat loads, and the importance of accurately capturing this effect justifies the inclusion of CEAM in the design problems.

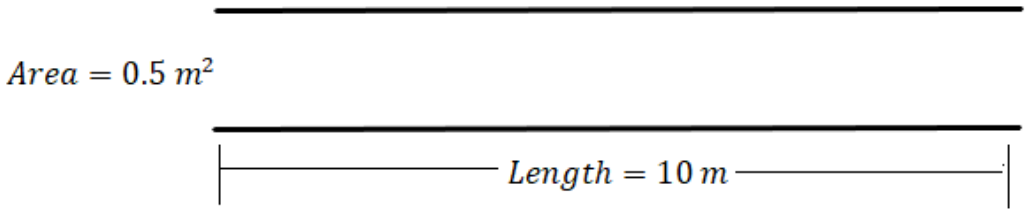

Figure 4.3: Fanno and Rayleigh Flow Test Case Geometry

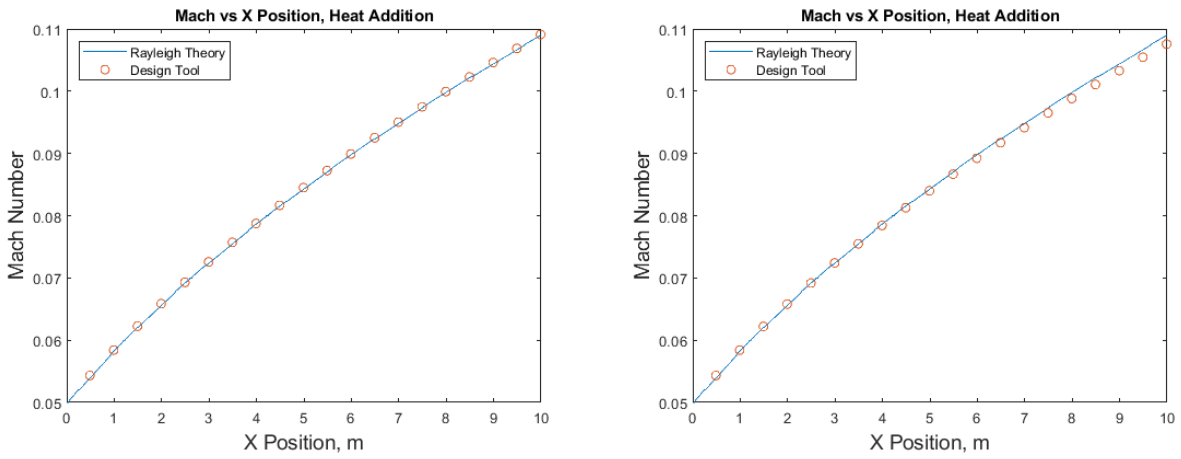

(a) Thermally Perfect Assumption (b) CEAM Calculated Properties

Figure 4.4: Flows with Heat Addition

4.1.3 Flow with Friction

Fanno flow is that in which the change in properties, including Mach number, are driven by the friction between the flow and the wall of the pipe. The same geometry as the Rayleigh test case was used for this test as well, with the total inlet temperature of $273K$ and an inlet total pressure of $101.3kPa$. The entry Mach number was once again $M = 0.05$. The friction factor was assumed to be a constant value of 0.5. For design problems, the friction factor is calculated from the flow state. That is done using an established correlation. The accuracy of the design tool in handling friction in the flow can be analyzed in isolation, as was done here. The friction factor would vary in the design problem, but otherwise the analysis method is the same. The results for Mach vs. X position were plotted and appear in figure 4.5.

The average error was calculated to be 0.01%. This low value is expected as the equations used in the model simplify out to essentially match the equations used for Fanno Flow. This level of error supports the accuracy of the numerical scheme employed, along with the sufficiently small value of Δx for the conditions present in this problem.

4.2 Δx Study

Serious consideration must be made for the value of Δx used for each case. The initial value used for the above problems was $0.001m$. This value was expected to be sufficiently small to capture the expected flow behavior, especially in cases with small and gradual changes in driving properties. For the purposes of verification, a comparison was done between the properties calculated using various values for Δx. The geometry used was generated in the design process for the simulator facility and includes the effects of heat transfer, a changing area, and friction with the walls of the pipe. This geometry was run with a range of values for Δx, and the program was timed during each run. The results of this study are summarized in table 4.1. The highest step count tested was 5000, correlating with a Δx value of $0.0001m$. The values for percent error were calculated using this 5000 point solution as the "true" value. Even the 250 point solution has a sufficiently low error for this particular case. However, the flow case analyzed does not include injected flow or particularly high temperature gradients,

so the step size may need to be smaller for those more complex cases. It is important to note that the error values shown are percentages, and while they begin to rise after the 250 point case, this is likely an effect of the linear interpolation used to compare points more than a true error in the results.

4.3 Execution Time Considerations

A major consideration with the design tool is the amount of time required to solve a given problem. The design tool itself was created to allow for rapid testing and design iterations so the time required to run the tool is a serious concern. The number of points modeled has the largest effect on execution time, which is something experienced in all numerical problems. The calculation steps themselves take very little time, but the call and execution of CEAM to calculate properties at each cell takes time. Originally, the execution time for 1000pt problems was on the order of three minutes. Improvements were made with the removal of a printing step that had been used for debugging. The execution time reduced, but there are still two calls made to the CEAM code each iteration. The value of Δx directly affects the number of iterations, as seen in table 4.1. This correlation increases the importance of balancing accuracy with computational cost.

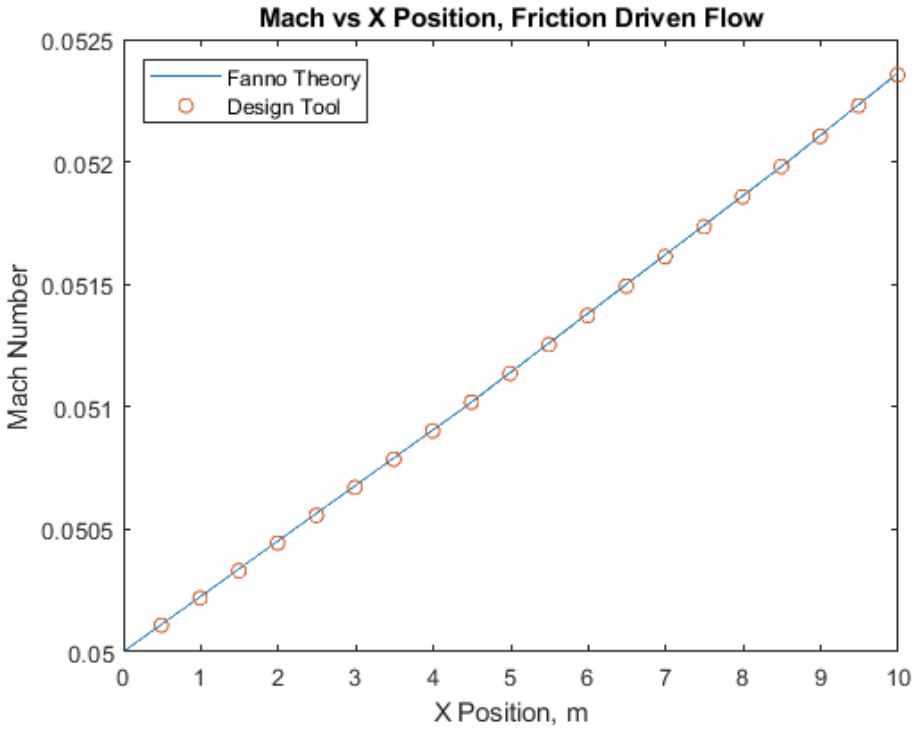

Figure 4.5: Mach vs. X Position, Friction as the Driving Function

Table 4.1: Δx Study

.

Number of Points	Δx (m)	Average % Error	Execution Time (s)
50	0.0103	0.03488	3.2
250	0.0021	0.00027	11.1
500	0.0010	0.00051	19.8
1000	0.0005	0.00069	39.3
2500	0.0002	0.00070	95.4
5000	0.0001	-	190.5

Chapter 5

Results and Discussion

The design tool has now been framed in a historical context and the operating theory behind it explained at length. The tool was created for a specific application, that of the creation of a baseline design for a nuclear thermal propulsion simulator. This application served both as a motivation for this work and a proof-of-concept of the design tool. The overall project goal is to create a facility that can be used to test different configurations and designs of core for a NTP system without the risks and complications brought on by the use of real nuclear material. Instead, resistive heating elements are used to simulate the fuel rods and achieve similar temperatures and thermal power levels in the core. This will allow for risk-reducing experiments to be performed that help guide and inform the design of a flight-ready system. The core design itself would be left to the contractors working on the flight system design, so the overall facility would need to be flexible enough to handle the various core layouts.

Regardless of the specific core design used, the target temperature at the outlet would be similar. This is because the temperature is directly related to the performance of a propulsion system. The concept of specific impulse was mentioned in Chapter 2. The simplified form of the I_{sp} equation previously introduced can be used to estimate the exhaust temperature required to reach a target performance for a given propellant composition.

$$I_{sp} = \sqrt{g_0 \frac{R}{mw} T_c} \tag{5.1}$$

The dependence on molecular weight encourages the usage of the lowest molecular weight propellant possible, which is hydrogen. In addition to the light weight, hydrogen has an advantage of decades of use as a propellant in liquid fueled rockets and the experience brought by this history. Once a propellant has been selected, a target I_{sp} must be chosen. For this facility, an I_{sp} of 900s was selected. This was motivated by many factors, the primary being a balance between improved performance and achievability. With this value in mind, the target exhaust total temperature at the exit of the core was determined to be approximately $2800K$.

Hydrogen at this temperature must be carefully controlled, as exposure to any atmospheric oxygen will result in autoignition and combustion of the gas. For this reason, the core flow must be cooled before being exhausted out of the system to the ambient atmosphere. The piping that carries the flow away from the core must be properly cooled itself to prevent failure, as must anything in the flowpath. The specific temperatures experienced, required cooling flows, and geometry of the downstream piping were all parameter that the design tool was created to investigate. In doing so, more accurate values could be provided to contractors and project sponsors, therefore enabling further design work to be completed. In this way, the design tool supports further development and enables more accurate communication with all stakeholders in the facility design.

5.1 Baseline Design

The original concept for the facility was explained in a white paper created for the project by Moeller et al in 2019 [38]. The main idea was to provide a platform for risk-reducing experiments that was both more affordable and more timely than alternatives. At the time of the original proposal, the time frame for the development of a flight-ready NTP system was considerably compressed. This motivated several design decisions made concerning engineering complexity. The original I_{sp} was considerably lower than 900s, but the overall facility design is similar. An updated proposal was produced in 2021 [39]. The facility design had been slightly modified, and an overview image of the updated concept is included as figure 5.1.

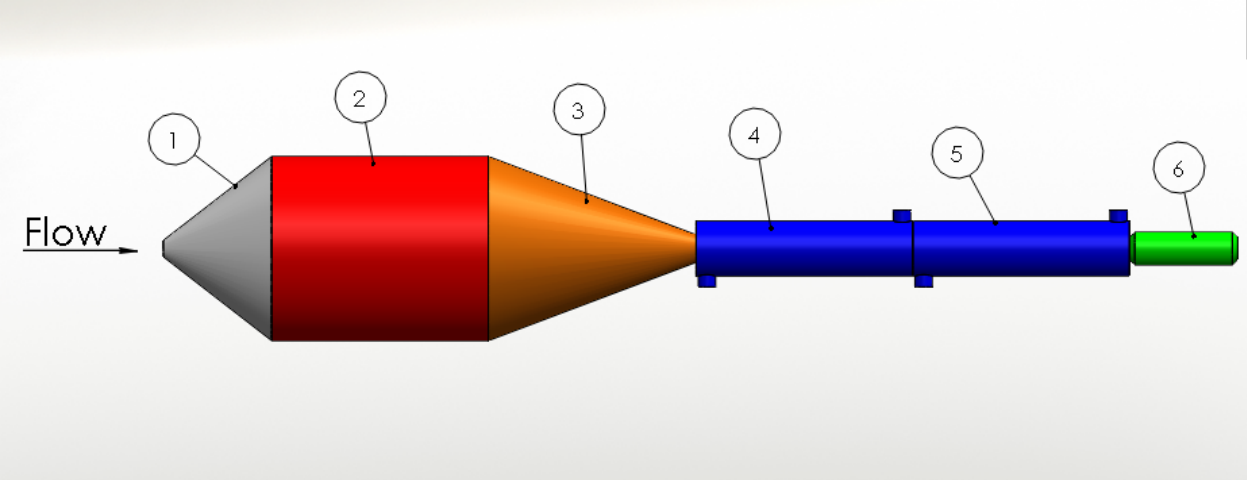

Figure 5.1: Schematic of Non-Nuclear Simulator Facility

The specific components highlighted are:

1. Inlet Plenum
2. Simulated Core
3. Exhaust Plenum
4. Water Injection Section
5. Heat Exchanger or Additional Water injection
6. Backpressure Device

The exhaust of the core section is assumed to be at a total temperature of $2800K$ at a core operating pressure of $150psi$. Additionally, the total mass flow through the system is assumed to be $0.2kg/s$ of hydrogen. The core internal diameter is $0.8m$. For the purposes of the design problem, the core was assumed to act as a "black box", with the flow out at the defined conditions but the specific core configuration left as an unknown. This reflects the flexible nature of the simulator, where specific configurations may vary between tests. Therefore, the design effort was focused on the portion of the facility downstream of the core, components 3-6.

5.1.1 Design Process

Initially, there were few design constraints which led to difficulty narrowing down the specifics of a configuration. The constraints that were introduced were cost and ease of construction. There was also a physical constraint limited to the building that the proposed facility was to be installed in. This limited the overall length of the facility. The flow rate within the facility was determined using NASA guidelines for the release of hydrogen to atmosphere [40]. It was known that the autoignition temperature of hydrogen was approximately $773K$, so it was known that the exhaust temperature must be below that value as well. The use of standard materials and dimensions was also desired to help keep costs low. Several high-temperature alloys exist that may be able to handle the temperatures experienced in exhaust system, but some cooling system was required to reduce the temperature of the hydrogen before it was

exhausted. For that reason, it was decided to also cool the exhaust structure in the same manner, therefore allowing for more common materials to be used in the design.

Stainless steel 316 was selected as the representative material for the flow passages in the exhaust structure design. It is commonly used in corrosive environments for chemical transport, and exhibits good resistance to the phenomenon of hydrogen embrittlement, a serious concern when working with hydrogen gas[41]. Sources vary on the maximum operating temperature of this material, but all fall within a range of $1088K - 1193K$ [42] [43]. The lower end of this range was selected to ensure that the cooling, as designed, could handle the worst case for the facility. This value of $1088K$ and was used for the wall temperatures within the cooled portion of the system.

5.2 Highlighted Components

Following the design process, the initial configuration of the exhaust system included three primary components. These were the exhaust plenum, the water injection portion, and a backpressure orifice. Each component utilized different abilities of the design tool. Flow in the exhaust plenum was mainly affected by the area change and heat transfer through the walls, and the mixing section had mass injection. The backpressure system required choked flow from the system as well.

5.2.1 Exhaust Plenum

The first component in the exhaust system is the exhaust plenum. It serves to reduce the diameter from the core down to the smaller diameter piping used for the rest of the exhaust. This is done for multiple reasons including the lower cost of smaller diameter piping and a smaller overall dimension for the system. The downstream diameter was selected to be $8in$. This diameter of pipe is large but still available as a standard size. The half angle for the converging plenum is 30 degrees. The resulting geometry is $0.528m$ long. The material used was assumed to be 316 stainless steel, and the wall temperature was assumed to be at the material limit of $1088K$.

The inlet conditions were assumed from the core flow exit conditions. The inlet total pressure was 1,034,000 kPa, or 10.3 bar. The inlet total temperature was $2800K$. The mass flow rate was $0.2kg/s$. Knowing the inlet diameter of $0.8m$ along with the flow rate and total temperature allowed for the calculation of an inlet Mach number of 0.001192.

The inlet Mach number was found through an iterative process. At the elevated temperature of the core, the heat capacity, C_p, of the flow is strongly affected by temperature changes. Additionally, the static temperature of the flow changes with Mach number. A script was created to determine the inlet mach, updating the value of C_p using CEAM. The process was as follows: First, a value was assumed for the inlet Mach number. Then, a value for the ratio of specific heats, γ, was also guessed. The temperature was calculated using the assumed Mach number and γ, then the equilibrium value of γ at that temperature was found using CEAM. If this was within a small allowance of the previous value, then the solution was considered converged. Otherwise, the value for γ was updated with the new calculated value. Once the temperature and γ were found for a given Mach number, the speed of sound and resulting mass flow rate was found. If the mass flow did not match the expected inlet value, a new Mach number was guessed and the process repeated.

Once the inlet conditions were determined, the exhaust plenum was analyzed using the design tool. The values most important from an analysis standpoint were the Mach number, pressure, temperature, and heat transfer through the wall. The design tool outputs a .txt file that contains the relevant flow properties at each location within the geometry. The results can then be plotted with relative ease, as was done below for the exhaust plenum. The output can then be used to design the support infrastructure and the downstream components. In order to help better visualize the flow as it passes through the geometry, the post-processing routine also generates a color contour plot of the variable in question for the geometry. This image is similar to the output generated by commercial CFD programs, and is done for many of the same reasons. This color plot for the Mach number within the exhaust plenum is presented in Figure 5.2a

From an initial Mach number of 0.001192, the flow accelerates to a Mach number of 0.01826 at the exit of the exhaust plenum. The overall change is small and leads to small changes in temperature and pressure. These results are acceptable and expected, as the

exhaust plenum is meant primarily just to reduce the overall diameter. The low Mach number at the exit is well below the choking condition which prevents the mass flow from being limited upstream of the orifice plate, which is specifically designed for the target mass flow rate. The Mach number, temperature, and pressure plots all demonstrate a similar trend. This is due to the change in area varying as a function of radius to the second power. A plot of cross-sectional area vs. position, shown in figure 5.4, was created and reflects this trend as well. The plots are exaggerated to allow small overall changes to be discerned.

An important consideration in these calculations is the required cooling for the system components. The hydrogen flow within the exhaust plenum is well above the maximum operating temperature of the stainless steel that the plenum is made from. In order to keep the interior wall from melting, water would be used as a heat sink. This would be done by circulating water through channels machined into the wall of the plenum. This is similar to a technique used in chemical rocket engines called regenerative cooling, where the heat extracted from the engine walls is used to preheat fuel before it is burned. However, the water here would be circulated out of the system, either to be cooled for immediate reuse or released to the environment. The exhaust plenum functions as a heat exchanger and could be modeled as such. However, the heat transfer is instead modeled as that between a fluid and a flat plate at constant temperature. This was done to make the analysis as applicable as possible to a wide range of geometries and provides a first-pass estimation of heat transfer. More accurate equations exist that account for the wall angle and model the heat exchange between the core and cooling flows more accurately, but would make the tool applicable to a more limited number of situations.

This idealized calculation ignores the temperature increase that would occur in the cooling flow as it absorbed heat transferred out of the hydrogen flow. In a true system, where the water is only flowing through the cooling channels, the water flow required would likely be higher in order to facilitate the heat transfer rates required. As the cooling flow temperature increased, higher convection coefficients would be needed to remove the same amount of heat. A higher-than-calculated mass flow rate of cooling water would lower the overall temperature of the cooling flow and would help maintain a high temperature difference and therefore, a high cooling rate. Additionally, the wall temperature in an operational system would vary

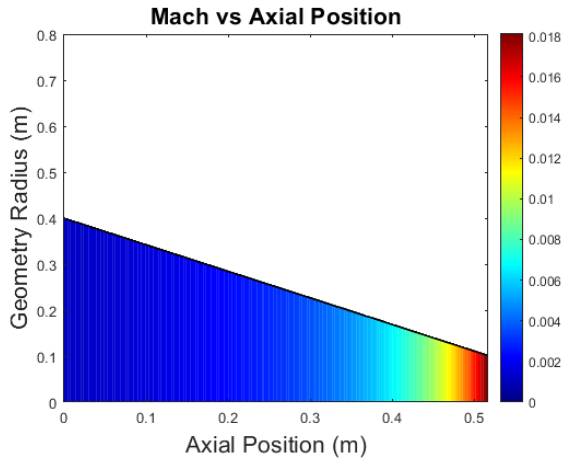

(a) Mach vs. Position Visualization

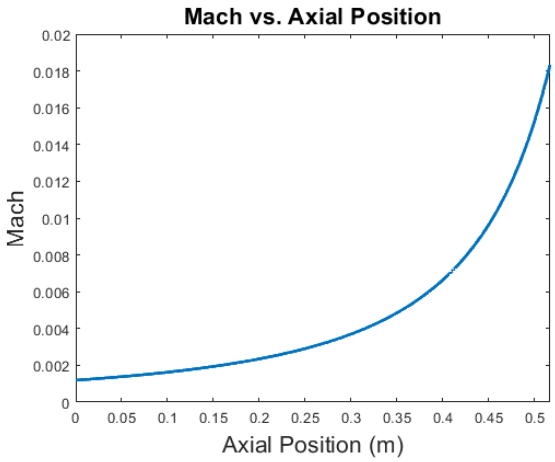

(b) Mach vs. Position Plot

Figure 5.2: Mach Number in the Plenum

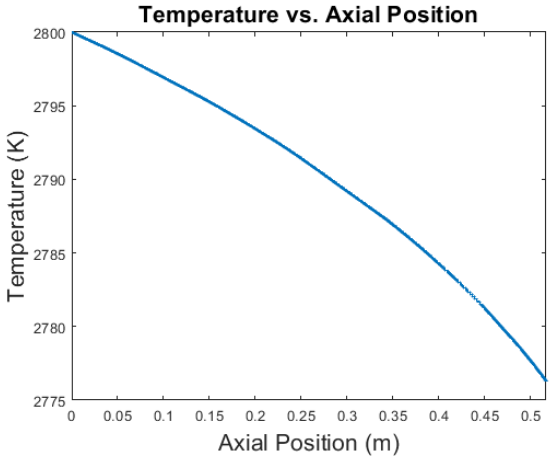

(a) Temperature Vs. Position

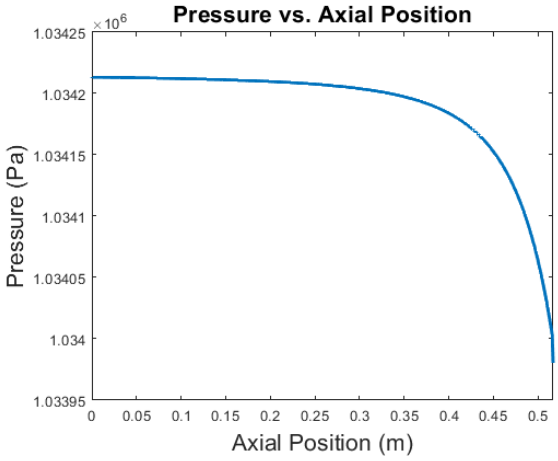

(b) Pressure Vs. Position

Figure 5.3: Plenum Properties

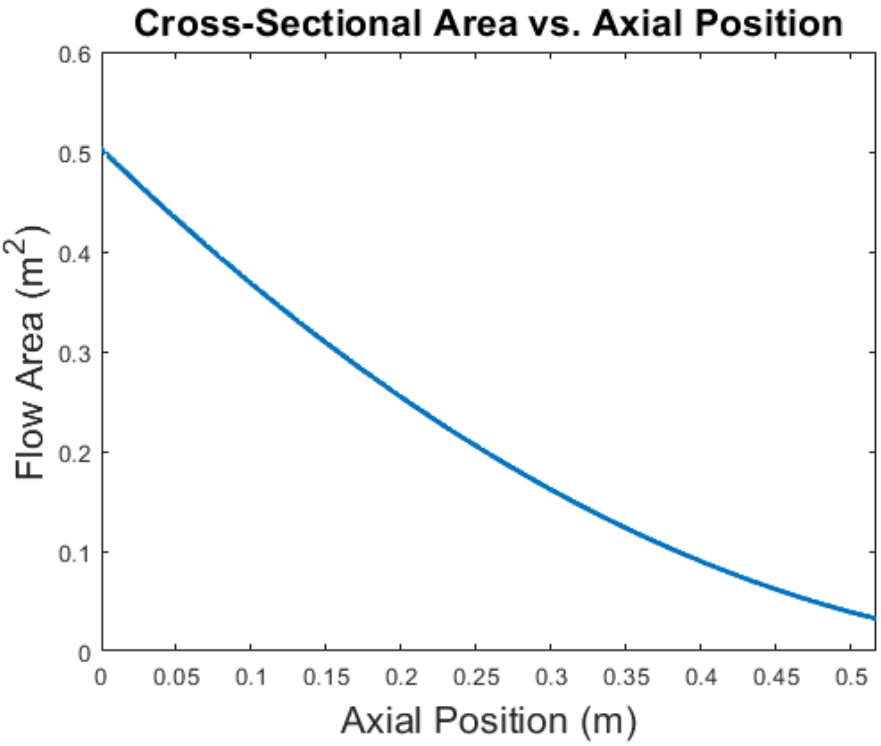

Figure 5.4: Area vs. Position, Exhaust Plenum

with axial position as the cooling flow would likely be injected at one end of the plenum and drawn off at the opposite end. If this temperature distribution of the wall was calculated, it could be entered back into the design tool to get an updated estimate of the heat transfer rate. This would be an iterative process, as the change in heat transfer rate would affect the cooling flow temperature in turn. The estimation completed here is aimed primarily at analysing the results of the cooling on the hydrogen flow within the system, so the cooling channel design was not analyzed in depth.

Total Temperature due to heat transfer agrees with the heat transfer rate through the walls. For cooling flow, the total mass of water required was calculated. Several assumptions were required to calculate the water flow required. The change in total temperature of the hydrogen flow was $23.62K$. Dividing this value by the average C_p and mass flow gives a total heat transfer out of the flow of $203{,}400W$. The amount of water required to absorb this energy can be calculated by dividing the total heat by the average C_p of water and the permitted temperature change. For water under atmospheric conditions, the boiling point is approximately $373K$. Raising from a room temperature value of $295K$ to boiling would results for a temperature change of 78 degrees. Using these assumptions, the mass flow of water required for just the exhaust plenum cooling is $0.62kg/s$, or $37.25L/minute$.

The inlet plenum design satisfies the design requirement of decreasing the diameter of the exhaust piping. In the functional facility, this section of the exhaust would also serve to collect the flow exiting individual channels within the core. This was not modeled within the testing as completed, but serves as yet another advantage of the use of this component.

5.2.2 Water Injection

The next component in the exhaust system is referred to as the water injection section. In the diagram, it is component 4. For this component, the geometry was decided based on several factors. The basic concept was a pipe with the inner wall covered in small holes through which water would be injected into the flow. The wall temperature was assumed to remain at the operating temperature of $1088K$, while the injected water was assumed to be at an initial temperature of 295K. This is approximately room temperature, and the water would be supplied from a tank either inside the simulator building or nearby outside.

This temperature reflects a reasonable assumption for ambient temperature of the reservoir during the test and neglects heat addition as the exhaust system is approached. It was desired that the internal diameter of the injection portion remain at 8 inches as this would increase ease in obtaining the pipe components for manufacture. An initial estimate of the total water injection required to lower the temperature to the target value was calculated using a heat balance and then divided by the surface area available for water injection on the inside face of the injection portion. It was assumed that 10% of the wall surface area was used to inject water. This value represents the amount of surface area occupied by the holes through which water flows to enter the core stream. The remaining 90% of the surface area would be normal piping and would require cooling. Heat transfer would occur across this remaining area.

The total water flow rate required for an exit temperature below the hydrogen auto-ignition temperature was estimated to be $2.0kg/$s. The area that this mass must pass through can be found by multiplying the total surface area by the percentage of area dedicated to the mass injection, in this case 10%. The injection velocity found using this method was much less than $1m/s$, assuming a $1m$ length for the injection section of the exhaust system. This calculation was done to ensure that the amount of water being injected into the flow within the $1m$ length was not unreasonable considering the geometry of the injector. In the production system, the holes would likely be much smaller to increase the flow velocity and achieve more of a "spray", but that design decisions will be left for later design work.

With this information, the flow within the injection section can be modeled. The mass injection through the wall is modeled as a constant injection of $2kg/s$ per meter of length, so each linear step in this length accounts for a small portion of this total flow. The water is assumed to be liquid and injected at the same pressure as the overall flow, at a temperature of $295K$. The effects of the change in total temperature due to the water injection are accounted for using CEAM. Plots of temperature, pressure, and Mach number against linear position are included below as before, in figure 5.5 and figure 5.6.

As expected, the Mach number increases as more mass is injected. The overall temperature decreases significantly and the increase in mass flow is the dominant factor for this change. An important note is the unusual behavior for temperature between the

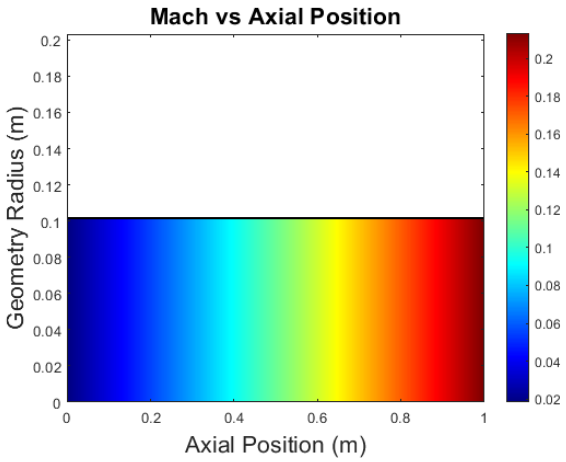

(a) Mach Vs. Position

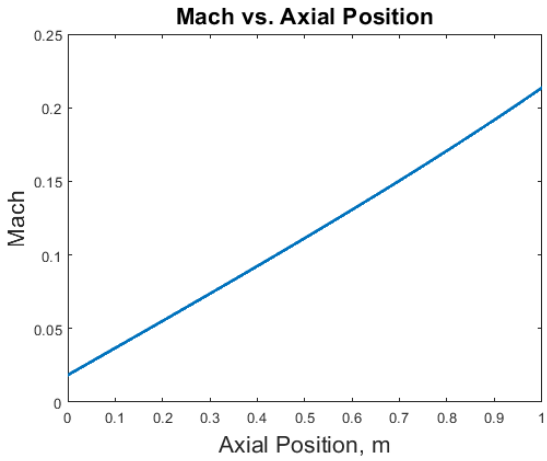

(b) Mach Vs. Position

Figure 5.5: Mixing Section Mach Number

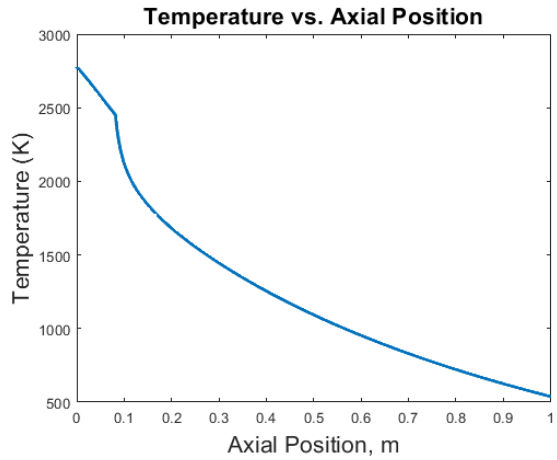

(a) Temperature Vs. Position

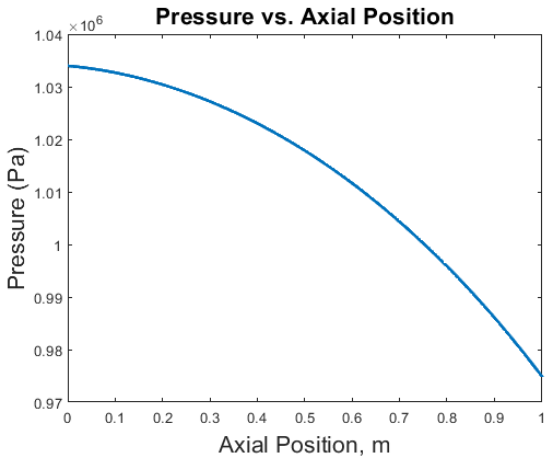

(b) Pressure Vs. Position

Figure 5.6: Mixing Section Properties

axial positions of 0 to $0.1m$. This is related to an issue discovered while working with the design tool. When mass flow is injected at a different temperature from that of the primary core flow, the effects of the temperature change are not fully captured. It is likely that the specific method of CEAM implemented in this model is not accounting for the dissociation of the injected fluid properly. This issue was discovered when comparing the actual mass flow present to the mass flow calculated from the exit Mach number and chemical properties of the exit flow. At the time of writing, work is ongoing to correct this issue. However, this issue is not expected to have a substantial effect on the solution and its applications to the design problem.

The water injection section is the final component for which water cooling is required, since the downstream temperatures are below the maximum operating temperature of the stainless steel pipe. Therefore, the total required cooling water for the system could be estimated once the deign of this component was complete. The water injection rate was added with the water flow required to cool the walls of the injection section. Using the same water properties as used in the exhaust plenum calculation, it was found that an additional $47{,}676J/s$ were removed from the flow through the wall. This would require an additional $0.145kg/s$ of cooling water, which brings the total required flow to approximately $2.75kg/s$. For a representative run time of 20 minutes, this would require approximately 900 gallons of water total. This is a worst-case calculation, where none of the water used for cooling the interior walls of the mixing section is injected. Even under these calculation conditions, a standard 1000 gallon water tank would provide an acceptable amount of water for each run.

5.2.3 Backpressure Orifice

Component 5, the heat exchanger, was removed from the design following the design process. It was found that the flow was not likely to choke within the water injection section at the mass flow rates required for proper cooling. This allowed for all of the required temperature reduction to be accomplished with the water injection alone. The removal of a heat exchanger reduces the cost and complexity of the overall facility.

As the flow total temperature was below the maximum operating temperature of the stainless steel, cooling was no longer required downstream of the water injection section.

This simplified the design of any downstream piping for the system. The final problem for the exhaust system to handle was the pressure differential. The exhaust flow is assumed to operate at a total pressure equivalent to that experienced in the core in the components listed thus far. However, the simulator will eventually exhaust to atmospheric pressure. A solution was required to limit the mass flow in the system and to support the large pressure differential.

In industrial applications, orifice plates are used to measure the mass flow rate within a pipe [44] [36]. In these applications, care is taken to minimize total pressure losses and prevent the mass flow rate from choking. However, an orifice plate can also be designed to intentionally limit the total mass flow through a pipe. In this application, the orifice is referred to as a restriction orifice [37]. Several methods exist to determine the orifice dimension appropriate for a target flow rate. A standard calculation method is provided by the International Organization for Standardization, or ISO. Their method is used and cited often in industrial design [45]. For a maximum reduction in pressure, the orifice should be designed so that the flow passing through it will choke. This occurs when the flow reaches a Mach number equal to 1.

If the orifice is sufficiently small enough to choke the flow within the plate, the total mass flow through the system will be limited to the choked condition. Once choked, the flow rate will not increase regardless of an additional drop in downstream pressure. The ratio between upstream and downstream pressures that causes choked flow is referred to as the critical pressure ratio, and for isentropic conditions can be calculated as a function of the ratio of specific heats, γ. For the flow exiting the mixing section, the γ is 1.43, which results in a $P_{crit} = 0.538$. Therefore, as long as the downstream pressure is below $540{,}500Pa$, the orifice will choke and the flow rate will be limited to a maximum target value of $2.2kg/s$.

For the purposes of design analysis, a small converging section was used to model the effect of an orifice on the flow. An initial guess for orifice size was made using the isentropic flow equations. At steady state, only wall friction and the area change are affecting the flow so the isentropic calculation should provide a fairly accurate approximation. The final diameter was found to be $0.1204m$. The Mach number at the orifice exit was 0.98. The accuracy of the design can be improved by adding in a sonic point handling function into

the design tool that would introduce limiting values as the local Mach number approaches 1, but as this was simply a representative design, it was omitted for now. The orifice plate used in the system would be designed according to the ISO standard for such devices, ISO [45], but this representation supports the use of such a device.

Plots are included below for the Mach number, pressure, and temperature through the converging section of the exhaust system. The plots again reflect the changing flow area and exaggerate the relatively small, over all changes to be readily seen. The flow is expected to choke at the outlet. Downstream of the plate, a supersonic jet is expected to occur. The flow will return to subsonic as a series of shocks and expansion waves occur in a diffuser, and the downstream flow will continue on to exhaust to the atmosphere. The remainder of the exhaust is a relatively simple pipe, the design of which will be left to later work.

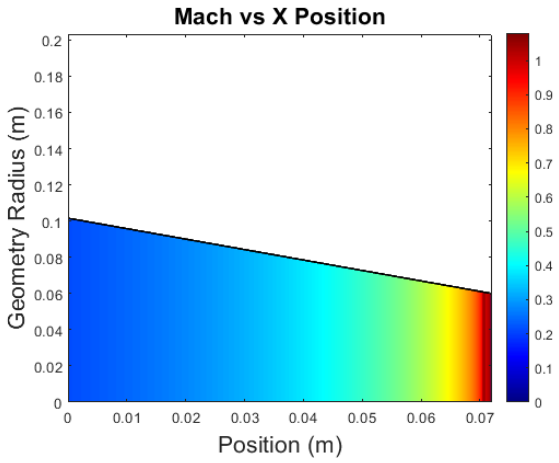

(a) Mach Vs. Position Visualization

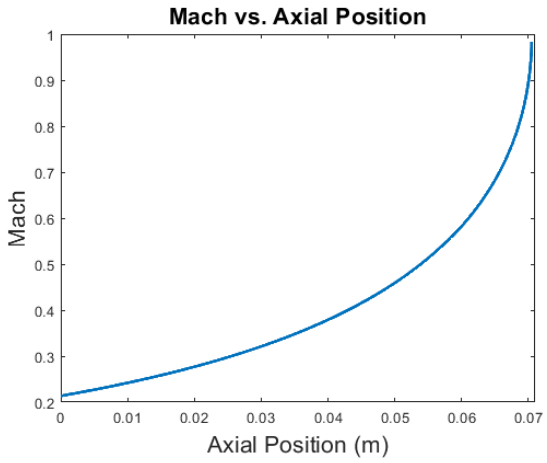

(b) Mach Vs. Position Plot

Figure 5.7: Orifice Plate Properties

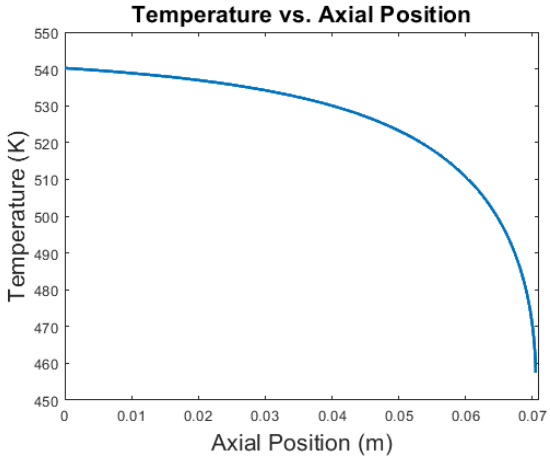

(a) Temperature Vs. Position

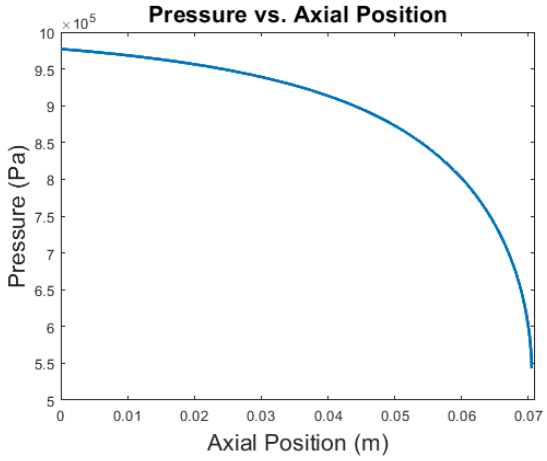

(b) Pressure Vs. Position

Figure 5.8: Orifice Plate Properties

Chapter 6

Conclusion

6.1 Summary

Nuclear thermal rockets are a promising technology for enhanced deep space access. The improvements in I_{sp} achievable with these systems greatly lessen the travel time for planned missions and enable new ones. While a proven concept, no NTP system has ever been flight tested. Prior work informs many of the present-day concepts, but any new system would require intensive ground-testing to refine the design before launching to space. Prior testing efforts were conducted with full-scale systems loaded with nuclear fuel, but present day environmental and political concerns would make such testing costly and difficult.

For these reasons, a non-nuclear simulator concept was proposed. The purpose of this simulator would be to allow for risk-reducing testing to be completed on multiple core configurations. Additionally, having a source of hydrogen at flow rates and temperatures present in a flight system could allow for component level testing or other expanded capabilities. This facility would be unique both in the power required and in its specific configuration.

In order to inform and guide the design process, a method was required to solve for the flow conditions within the proposed configurations. A design tool was created for this purpose based on quasi-one-dimensional flow analysis. The tool was designed to account for the effects of mass injection, wall friction, heat addition or removal, and changing area. The addition of a chemical equilibrium code to the design tool allowed for the tool to analyze flows

at high temperatures, where the chemical properties are no longer constant. The specific code utilized, CEAM, calculated the percent of hydrogen that dissociated and the properties of the mixture at each linear step. The equations used for this method are derived from conservation laws and assume constant properties within each individual cell. The resulting differential equation defining the effect of each driving function, including the changing flow area, mass injection, wall friction, and heat transfer, on the Mach number of the flow is numerically integrated using the fourth-order Runge-Kutta technique. The temperature, pressure, and other properties are solved for using integral relations based on the changing Mach number. This method allowed for the flow conditions to be found throughout the analyzed geometry. A series of test cases with known analytical solutions was used to validate the design tool.

Once the flow state within a component is known, the results can be analyzed and compared with other design concepts. This analysis allows for rapid design comparisons and refinement. The design tool was used to create an initial configuration for the exhaust system. This system serves to cool the flow below the autoignition point of hydrogen and to provide the backpressure to the system that would be created by a nozzle in flight. This solution serves both as example case of use for the design tool and as a starting point for further development of the simulator facility.

6.2 Future Work

While the design case for this work has been focused on a conceptual facility, the same analysis techniques used for this work can and have been employed to analyze other flow situations. With the addition of a shock-handling portion, the design tool could be used to analyze supersonic internal flows. This would open many more potential applications. For example, a blow-down supersonic wind tunnel could be analyzed in its steady-state condition to determine the effects of heating on the flow. Initial sizing of components and determination of mass flow could be accomplished quickly.

Simple combustion could be readily modeled within the flow as well. CEAM can accept multiple input species and will calculate the output equilibrium flow state including the effects of combustion. This would allow for simple burners to be modeled. Another possibility

is the addition of a heat exchanger model to the design tool. If enough information is known or can be assumed about the flow of a cooling fluid, the wall temperature could be found dynamically as opposed to remaining a constant value. This would allow for the integrated effects of cooling to be modeled, and provide more information to the design team.

The most important next step for the design tool is to address the shortcomings regarding the modeling of injected flow. While the mass injection is properly captured, something within the tool is causing an over-prediction of mass flow when a cooling flow is injected. This behavior does not occur when fluid of a different species is injected into the core flow at the core flow temperature, but rather only presents itself when two fluids of different temperatures mix. This problem is likely due either to the specific method in which CEAM is used to determine flow properties, or by an inaccurately applied assumption of constant chemical properties within the differential volume of each cell. The later may require either much smaller cell sizes or the use of more general equations to be solved. This an area of ongoing work.

Once refined, the fidelity of the tool could be increased by several methods while still remaining computationally inexpensive. An optimization of the heat transfer equations used, for example, would allow for a better estimation of the heat flowing out of the system in a converging geometry. Modeling the cooling flow could also be done to provide more useful and accurate results from the tool. The core of the reactor could be modeled as well if a temperature distribution was determined or calculated for the heating elements. A change to the non-constant properties form of the derived equations may prove useful for modeling complex flows more accurately, but would again increase complexity and computational expense of the tool. The benefits of increased fidelity must be weighed against the cost of increased complexity for each flow analyzed. The implementation of the design tool and the methods by which it simulates the flow as presented in this thesis serve as a starting point for more complex designs and applications.

Bibliography

[1] Fishbrine, B., Hanrahan, R., Howe, S., Malenfant, R., Scherer, C., Sheinberg, H., and Ramos Jr., O., "NUCLEAR ROCKETS: To Mars and Beyond," *National Security Science*, Vol. 1, 2011. URL https://www.lanl.gov/science/NSS/issue1_2011/story4full.shtml. 1, 10, 11, 12, 13

[2] "SSME: Space Shuttle Main Engine," Pratt & Whitney Rocketdyne, 2005. URL http://www.pw.utc.com/products/pwr/assets/pwr_SSME.pdf. 2

[3] Dodd, T., "Is SpaceX's Raptor engine the king of rocket engines?" Everday Astronaut, 2019. URL https://everydayastronaut.com/raptor-engine/. 2

[4] Tucker, J., "SpaceX's Raptor isn't the only new propulsion system out there..." Medium.com, 2019. URL https://medium.com/newspace-hub/spacexs-raptor-isn-t-the-only-new-rocket-engine-out-there-fb3b68e3a939. 2

[5] Arbit, H., Clapp, S., and Nagai, C., "COMBUSTION CHARACTERISTICS OF THE FLUORINE/LITHIUM/HYDROGEN TRIPROPELLANT COMBINATION," *AIAA 4th Propulsion Joint Specialist Conference*, Cleveland, OH, 1968. doi:10.2514/6.1968-618. 2

[6] Robbins, W., "An Historical Perspective of the NERVA Nuclear Rocket Engine Technology Program," *AIAA/NASA/OIA Conference on Advanced SEI Technologies*, AIAA, Cleveland, OH, 1991. doi:10.2514/6.1991-3451. 2, 5, 12

[7] Houts, M. G., Kim, T., Emrich, W. J., Hickman, R. R., Gerrish, J. W. B. H. P., and Doughty, G., "The Nuclear Cryogenic Propulsion Stage," *AIAA Propulsion and Energy Forum*, American Institute of Aeronautics and Astronautics (AIAA), Cleveland, OH, 2014. doi:10.2514/6.2014-3724. 3

[8] Emrich Jr., W., *Principles of Nuclear Rocket Propulsion*, Butterworth-Heinemann, Cambridge, MA, 2016. 3, 6, 13, 15

[9] Sievers, R., Livingston, J., and Pierce, B., "NERVA Propulsion System Design Considerations," *AIAA/SAE/ASME/AEEE 26th Joint Propulsion Conference*, Orlando, FL, 1990. doi:10.2514/6.1990-1951. 3

[10] Ebersohn, F. H., Longmier, B. J., Sheehan, J. P., Shebalin, J. V., and Girimaji, S. S., "Preliminary Magnetohydrodynamic Simulations of Magnetic Nozzles," *33rd International Electric Propulsion Conference*, The George Washington University, Washington, DC, 2013. 4

[11] Emrich Jr., W., "Figure 4.6 Minimum Transit Times Between Earth and Mars," Interactive Figure, Elsevier, 2016. URL https://booksite.elsevier.com/9780128044742/interactive.php. 4

[12] Haslett, R. A., "Space Nuclear Thermal Propulsion Program," Report PL-TR-95-1064, Grumman Aerospace Corp, Bethpage NY, May 1995. 5, 10, 14, 15

[13] Werner, J., Bhattacharyya, S., and Houts, M., "An Overview of Facilities and Capabilities to Support the Development of Nuclear Thermal Propulsion," *Nuclear and Emerging Technology for Space*, Albuquerque, NM, 2011. URL https://www.osti.gov/servlets/purl/1013713. 5

[14] Holman, R. R., and Pierce, B. L., "Development of NERVA Reactor for Space Nuclear Propulsion," *AIAA/ASME/SAE/ASEE 22nd Joint Propulsion Conference*, Huntsville, AL, 1986. doi:10.2514/6.1986-1582. 5

[15] Johnson, P., "A Summary of Nuclear Rocket Applications," *1st Annual AIAA Conference*, Washington, DC, 1964. doi:10.2514/6.1964-388. 10

[16] Gerrish, H. P., "Nuclear Thermal Propulsion Ground Test History," *2014 Nuclear Emerging Technologies for Space Conference*, Pearlington, MS, 2014. 12

[17] Lyon, L. L., "Performance of (U,Zr)C-Graphite (Composite) and of (U,Zr)C (Carbide) Fuel Elements in the Nuclear Furnace 1 Test Reactor," Report LA-5398-MS, Los Alamos National Laboratory, September 1973. 13

[18] Wade, M., "Russian Mars Propulsion - Nuclear Thermal," Website, 2019. URL http://www.astronautix.com/r/russianmarsucleartherma l.html. 15

[19] Shapiro, A. H., *The Dynamics and Thermodynamics of Compressible Fluid Flow*, Ronald, New York, 1953. 16, 19

[20] Boylston, B. M., "Quasi-One-Dimensional Flow for Use in Real-Time Facility Simulations," Thesis, University of Tennessee, 2011. URL https://trace.tennessee.edu/utk_gradthes/1058/. 16, 17

[21] Beans, E. W., "Computer solution to generalized one- dimensional flow," *Journal of Spacecraft and Rockets*, Vol. 7, No. 12, 1970, pp. 1460–1464. doi:10.2514/3.30192, URL https://arc.aiaa.org/doi/abs/10.2514/3.30192. 17

[22] Beans, E. W., "Nozzle Design Using Generalized One-Dimensional Flow," *Journal of Propulsion and Power*, Vol. 8, No. 4, 1992, pp. 917–920. doi:10.2514/3.23572. 17, 19

[23] Birzer, C. H., and Doolan, C. J., "Quasi-One-Dimensional Model of Hydrogen-Fueled Scramjet Combustors," *Journal of Propulsion and Power*, Vol. 25, No. 6, 2009, pp. 1220–1225. doi:10.2514/1.43716. 17

[24] Picard, M., Rancourt, D., Plante, J.-S., and Brouillette, M., "Rim-Rotor Rotary Ramjet Engine, Part 2: Quasi-One-Dimensional Aerothermodynamic Design," *Journal of Propulsion and Power*, Vol. 28, No. 6, 2012, pp. 1304–1314. doi:10.2514/1.B34226. 17

[25] Saad, M. A., *Compressible Fluid Flow*, Prenctice-Hall, Inc., Englewood Cliffs, New Jersey, 1985. 19, 20

[26] Zucrow, M. J., and Hoffman, J. D., *Gas Dynamics*, 1st ed., Vol. 1, John Wiley Sons, Inc., New York, 1976. 19, 20, 21, 26

[27] Hodge, B. K., "Generalized One-dimensional Compressible Flow Techniques," *International Journal of Applied Engineering*, Vol. 7, No. 1, 1991, pp. 56–63. URL https://www.ijee.ie/. 19, 24, 25

[28] Anderson Jr., J. D., *Modern Compressible Flow: With Historical Perspective*, 3rd ed., McGraw-Hill Higher Education, New York, 2002. 19

[29] Hodge, B. K., "Mathcad applications for generalized one-dimensional compressible flow," *International Journal of Mechanical Engineering Education*, Vol. 39, 2011, pp. 139+. URL https://link-gale-com.utk.idm.oclc.org/apps/doc/A382279891/AONE?u=tel_a_utl&sid=bookmark-AONE&xid=7a2e8a61. 20, 28

[30] Petukhov, B. S., *Advances in Heat Transfer*, Vol. 6, Academic Press, New York, 1970. 28

[31] "Woods Reservoir," Website, Lakes Online, 2022. URL http://woods.uslakes.info/. 29

[32] Gnielinski, V., "New Equations for Heat and Mass Transfer in Turbulent Pipe and Channel Flow," *International Chemical Engineering*, Vol. 16, No. 2, 1976, pp. 359–268. 29

[33] McBride, B. J., and Gordon, S., "Chemical Equilibrium with Applications," Computer Program, NASA, 1996. URL https://software.nasa.gov/software/LEW-17687-1. 31

[34] McBride, B. J., and Gordon, S., "Computer Program for Calculation of Complex Chemical Equilibrium Compositions and Applications II. Users Manual and Program Description," Report NASA-RP-1311, Office of Management, Scientific and Technical Information Program, NASA, 1996. URL https://ntrs.nasa.gov/citations/19960044559. 31

[35] Kobliska, S., and Kopicz, C., "Chemical Equilibrium with Applications for MATLAB," Computer Program, NASA, 2017. URL https://software.nasa.gov/software/MFS-33320-1. 31

[36] Dey, A. K., "What is a Restriction Orifice? Applications, Types, Working, and Sizing of Restriction Orifices," Web Blog, 2020. URL https://whatispiping.com/restriction-orifice/. 32, 54

[37] "Restriction Orifice Plates," Solartron ISA, 2022. URL https://www.solartronisa.com/products/dpflow/restriction-orifice-plates. 32, 54

[38] Moeller, T., Davenport, J., Kraft, E., Davis, M., Kolwyck, J., McMinn, W., Goodman, J., and Jones, J., "Final Report for Non-Nuclear Simulator and Digital Engineering Concept Study for Nuclear Thermal Propulsion," , 2019. Unpublished Work. 42

[39] Clemons, E., Long, E., Moeller, T., Davenport, J., and Kolwyck, J., "Non-Nuclear Simulator Testing Facility for Nuclear Thermal Propulsion Research," , 2021. Unpublished Work. 42

[40] Ordin, P. M., "Safety Standard for Hydrogen and Hydrogen Systems," Report NSS 1740.16, NASA, 1997. 44

[41] Caskey Jr., G. R., "Hydrogen Compatibility Handbook for Stainless Steels," Report DP-1643, E. I. du Pont de Nemours Co., Aiken, SC, 1983. 45

[42] "Flat Product Stainless Steel Grade Sheet," Online Datasheet, North American Stainless, 2010. URL https://www.northamericanstainless.com/wp-content/uploads/2010/10/Grade-316-316L.pdf. 45

[43] "Corrosion-Resistant 316 Stainless Steel," Web Catalog, McMaster-Carr, 2022. URL https://www.mcmaster.com/browse-pipe-tubing,-hose-and-fittings/stainless-steel/material~316-stainless-steel/. 45

[44] "Orifices & Flows," Online Blog, Engineers for Engineers, 2021. URL https://engineersforengineers.com/2021/10/11/orifices-flows/. 54

[45] "Measurement of fluid flow by means of pressure differential devices inserted in circular cross-section conduits running full," Standard ISO 5167-2:2003, ISO, 2003. URL https://www.iso.org/standard/30190.html. 54, 55

Vita

Ethan Long grew up in Nashville before pursuing a Bachelor's Degree in Aerospace Engineering at the University of Tennessee. Following graduation, he moved to Tullahoma, Tennessee to pursue a Master's Degree at the University of Tennessee Space Institute, with a thesis focus in nuclear thermal propulsion. After graduation, he will begin position as a propulsion engineer at Ursa Major Technologies in Berthoud, Colorado conducting developmental testing of new engine designs. He is grateful for all of the support as he begins this next chapter in life.